

Non-invasive ultrasound measurements of vascular impedance

- Rekindling an old in-house concept on *in vivo* measurements -

Roger Larsson

Year: 2018



LUND
UNIVERSITY

Master's Thesis in
Biomedical Engineering

Faculty of Engineering LTH
Department of Biomedical Engineering

Supervisor: Magnus Cinthio
Deputy supervisor: Tobias Erlöv

“The opinion of the world does not affect me. I have placed as the real values in my life what follows when I am dead.”

Nikola Tesla

“The weed crushed and pressed by the heavy rock may slowly and gently grow up anew helped by the fresh air, sunshine and sympathetic rain. On the other hand, the rock is often broken through exposure to nature and weathering. Life is a strong power to grow in tenderness; this fact may be considered as having a close relation with human life. At the same time tenderness has sometimes stronger power against stiffness or hardening due to extreme strain.”

Kyozo Mifune

Abstract

Despite its introduction in the early 1950's, vascular impedance has yet to be applied in clinical use to predict early stages of cardiovascular disease (CVD). It is defined as the ratio between blood pressure and flow and describes the opposition to blood flow within the cardiovascular system.

During this thesis project, local pulse wave velocity (PWV) and vascular impedance was estimated from *in vivo* ultrafast plane wave imaging recordings of the right common carotid artery in eight healthy human volunteers. Both estimations were based on the tracking of the arteries radial displacement. Motion tracking was performed by using two tracking methods: phase shift (PS)- and iterative phase shift (IPS)-tracking. The IPS-tracking is a brand new radial motion tracking method on vessels created during this project by combining existing phase shift- and block matching motion tracking methods in use at the Department of Biomedical Engineering, Lund University.

Results showed local PWV-estimations to vary, occasionally to a substantial degree, between, as much as within, volunteer recordings. For the incident pulse wave, probable PWV values totally varied between 1.58 – 7.60 *m/s*. For the bifurcation wave reflection, probable PWV values totally ranged between 1.06 – 16.09 *m/s* in the opposite direction. The vascular impedance, defined as vascular characteristic impedance used to estimate vascular input impedance, was in partial successfully determined in two volunteers. The results, however, suggest both local PWV- and vascular impedance estimations to be sensitive to slope fitting of the progressive change in cardiac cycle locations and phase between consecutive scanlines. Furthermore, vascular impedance estimations seem to require longer *in vivo* recordings containing multiple heart cycles to gain more certain results.

Sammanfattning

Trots dess introduktion under början av 1950-talet används vaskulär impedans ännu inte i klinisk omfattning för att förutsäga tidiga stadier av hjärt-kärlsjukdomar. Definierad som förhållandet mellan blodtryck och blodflöde beskriver vaskulär impedans motståndet mot blodflödet i det vaskulära systemet.

Under detta avhandlingsprojekt uppskattades den lokala pulsvåghastigheten (PWV) och vaskulära impedansen från *in vivo* ultrasnabba planvågsbildningsinspelningar över den högra halspulsådern hos åtta friska frivilliga forskningspersoner. Båda uppskattningarna baserades på spårningen av artärens diametraliska rörelsemönster. Spårningen utfördes via två spårningsmetoder: fasförskjutning (PS-tracking) och iterativ fasförskjutning (IPS-tracking). IPS-metoden är en helt ny spårningsmetod för radiell rörelse hos kärl, skapad under detta projekt genom att kombinera befintliga fasförskjutnings- och block-matchande rörelsespårningsmetoder i bruk vid Avdelningen för Biomedicinsk Teknik, Lunds Universitet.

Resultaten visar på varierande lokala PWV-uppskattningar, i potentiellt väsentlig grad, mellan, såväl som inom, individuella forskningspersoners inspelningar. Den framåtgående pulsvågen uppvisade troliga PWV-värden mellan 1.58 – 7.60 *m/s*. För bifurkationspulsvågsreflektionen förekom sannolika PWV-värden mellan 1.06 – 16.09 *m/s* i motsatt riktning. Den vaskulära impedansen, definierad som vaskulär karakteristisk impedans men som används för att uppskatta vaskulär ingångsimpedans, bestämdes till största del framgångsrikt hos två forskningspersoner. Resultaten föreslår dock att både lokala PWV- och vaskulära impedansuppskattningar är känsliga för lutningsanpassningen efter den progressiva förskjutningen i hjärtcykelfas och fas mellan på varandra följande skanningslinjer. Vidare verkar vaskulära impedansuppskattningar kräva längre *in vivo* inspelningar med fler hjärtcykler, för att ge mer pålitliga resultat.

Preface

This thesis project was carried out during the spring and autumn terms of 2018 at LTH, Lund University. It has been an *in vivo* continuation of the Ph.D. thesis “*Development and evaluation of non-invasive ultrasonic methods for arterial characterization*” by **Anders Eriksson** at the Department of Biomedical Engineering (former Department of Electrical Measurements), Lund University. The aim has been to determine the vascular impedance inside the right common carotid artery.

Overall, I would like to give a warm thank you to the Department of Biomedical Engineering, Lund University, and its personnel. Thanks to the pleasant and familiarity atmosphere, I have always felt at home at your department; a feeling that should not be taken easily. With your open mindedness and enthusiastic teaching, you opened up my eyes to the field of Biomedical Engineering.

Especially, I would like to thank my two supervisors: **Magnus Cinthio** and **Tobias Erlöv**.

Magnus: Thank you for your never ending support, for believing in me and for giving me this rare and honourable opportunity. Your kindness, commitment, vast medical experience and never ending optimism never ceased to amaze me.

Tobias: Thank you for your never ending support, kindness and vast coding expertise. Thank you for letting me work next to you in “our” office. All of our deep and witty discussions, being both on- and off-topic, were always as amusing as they were stimulating.

Together, you have inspired me to pursue a research career on my own. In synergy with you as supervisors, I managed to pull off my most ambitious work to date. So ambitious in fact that we are now going to

compose and publish a letter together in a scientific journal based on our new tracking method. My hopes are that this project and all my labour will help you continue and support your research in the future. The project has been toilsome from time to time, but always fun and inspiring at the same time. This year has truly been a once in a lifetime experience which I will cherish for the rest of my life. Thank you for taking me under your wings and always encouraging me. It has been a true honour working alongside with you and I hope you enjoyed it as much as I did! To you, I will forever be grateful and in debt.

I would also like to thank all the other members of the department's ultrasound research team: *Monica Almqvist, Maria Evertsson, Hans W. Persson, John Albinsson, Sandra Sjöstrand, Josefin Starkhammar, Roger Andersson* and *Tomas Jansson*. Thank you for your warmth, your kindness and your openness; welcoming me into the group and making me feel at home. It meant a lot to me. If it weren't for you, and the ultrasound course you organize, I would probably not have ended up doing this thesis project or even pursued Biomedical Engineering in the first place. For that, I am forever grateful and I hope you enjoyed my company as much as I did to yours.

Through this master thesis project, I have gained friends for life. But even though this project now has come to an end, I don't see it as the end to our relations. I would gladly like to keep in touch with you and hope you allow me to continue accompany you on your weekly lunches every Thursday. That would be lovely!

Additionally, thank you *Axel Tojo* for all technical support and for setting up my workspace.

Also, thank you *Désirée Jarebrant* for assisting with all administrative work and entrusting me with a key to the office.

Lastly, I would like to thank my mother and sister for your patience and support during this thesis project and the education throughout.

Contents

1. Introduction	1
1.1 Background.....	1
1.2 Aim.....	3
1.3 Previous results and interest outside of the department	5
2. Theory	9
2.1 Ultrasound	9
2.2 Ultrasound imaging techniques	16
2.3 The circulatory system and its historical background	19
2.4 The arterial wall and its properties	25
2.5 Pulse wave velocity	34
2.6 Wave reflections	36
2.7 Vascular impedance.....	38
2.7.1 Terminology	38
2.7.2 Bringing vessel characteristics into an impedance model....	42
2.7.3 Units of impedance modulus.....	44
2.7.4 Longitudinal impedance	45
2.7.5 Characteristic impedance	48
2.7.6 Input impedance	52
2.7.7 Terminal impedance	55
2.8 Diagnosis from vascular impedance patterns	56
2.9 Input impedance as ventricular load and vascular power	60

3. Method.....	65
3.1 Pre-existing in vivo recordings.....	65
3.2 New measurements and beamforming	65
3.3 Motion tracking	67
3.3.1 Zero crossing–tracking.....	68
3.3.2 Phase shift–tracking	69
3.3.3 Iterative phase shift–tracking	70
3.3.4 Performance evaluations	73
3.4 Local pulse wave velocity estimations	74
3.5 Vascular impedance estimations	80
4. Results	83
4.1 Motion data.....	83
4.2 Performance evaluations.....	84
4.3 Local pulse wave velocity	91
4.3.1 Forward propagating pulse wave	91
4.3.2 Bifurcation wave reflection.....	96
4.4 Vascular impedance.....	103
5. Discussion.....	107
5.1 Measurements and in vivo recordings	107
5.2 Motion tracking and performance evaluations	108
5.3 Local pulse wave velocity estimations	110
5.4 Vascular impedance estimations	113
6. Conclusions	119
Bibliography	123

1. Introduction

1.1 Background

Cardiovascular diseases (CVDs) are today the most common cause of death in humans. Worldwide, 17.7 million deaths, 31 % of all global deaths, in 2015 were related to CVD. Future predictions estimate this number to increase in the future, with 23.3 million people deaths from CVDs in 2030 [1]. It is thus of considerable interest to detect symptoms of CVD at an as early stage as possible. Today, manual and automatic blood pressure measurements are used as a standard procedure to assess cardiovascular function in patients. Even so, blood pressure measurements are far from a perfect and precise measurement tool. Apart from being affected by measurement- and interpretation errors, they also give indication of disease first at a progressive state.

A new method of estimating the cardiovascular system health condition has previously been developed by the Department of Biomedical Engineering (formerly the Department of Electrical Measurement), Lund University, that utilizes non-invasive ultrasound technology to estimate pulse wave velocity (PWV) and vascular impedance frequency composition in blood vessels [2]. This is achieved by extracting and analysing the diametric displacement of vessels, caused by the radial motion of the upper and lower vessel walls during cardiac pulsation cycles. An illustration of the perpendicular movements present in vessels is seen in *Figure 1.1* below.

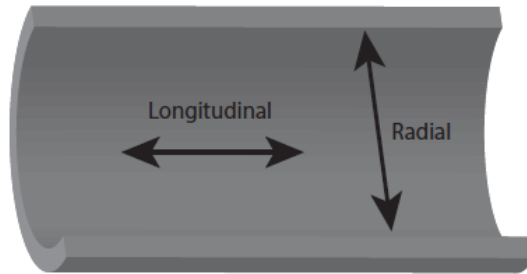


Figure 1.1: Illustration of longitudinal- and radial arterial movement. Used with permission from Sjöstrand S. [3].

The concept is traceable back to the late 1990's and has previously only been tested on tubes in the lab. The laboratory tests have shown promising results, but the technique has until now awaited technological maturity to be successfully implemented in a more clinical setting.

Vascular impedance is the resistance to flow in the cardiovascular system and corresponds to the work load to which the heart has to work against to circulate the blood around the circulatory system. Vascular impedance increases with reduced vessel size, being through e.g. natural diminution, presence of plaque or increased arterial stiffness. By measuring vascular impedance as close to the heart as possible gives a good indicator of the local- or global (depending on its definition) health condition of the cardiovascular system.

Related to vascular impedance is vascular power which corresponds to the effect by which the heart has to put out to circulate the blood through the systemic- and pulmonary circulatory systems. By estimating vascular power through non-invasive ultrasound technology opens up to the opportunity to non-invasively survey distribution of power within the branches of the arterial tree.

This method, due to its intended use in medical ultrasound equipment, enables lower risk of measurement- and interpretation errors. It also

enables diagnosis at an earlier stage of disease than other methods in today's clinical practice.

1.2 Aim

The purpose of this thesis project has been to continue on the Ph.D thesis "*Development and evaluation of non-invasive ultrasonic methods for arterial characterization*" by Eriksson *et al.* [2], a former department employee.

The overall aim of this thesis project has been (throughout) to determine the vascular impedance in the right common carotid artery from acquired *in vivo* ultrafast plane wave ultrasound recordings.

Initially, a set of recordings from the Skåne University Hospital (SUS), Malmö, were meant to be analysed. If successful, additional recordings would be collected, containing more data to also enable determination of vascular power within the right common carotid artery.

Since the project has been metrological (metrology = science of measurement) in nature throughout, the task was originally to further develop pre-existing techniques and algorithms to:

1. *Study and refine the pre-existing, but yet unpublished, tracking method created by Cinthio M. for motion tracking in radio frequency (RF)-data.*
2. *Further develop the tracking method in (1) to use the extracted motion data to estimate local PWV in the in vivo ultrafast imaging ultrasound recordings of the right common carotid artery.*
3. *Further develop the tracking method in (2) to determine phase velocity and vascular impedance in the in vivo recordings.*

4. *Potentially evaluate the developed methods performance through measurements on ultrasound phantoms.*
5. *Potentially combine the developed method in (3) and its measurement results with flow measurements to determine vascular power.*

However, these aims had to be changed due to early complications in the process. The pre-existing *in vivo* recordings were found inadequate in quality, as they seemed not to contain an incident pulse wave from the heart. New *in vivo* ultrafast ultrasound recordings had thus to be taken. Also, due to echo instability in the pre-existing recordings, the intended tracking method was found too sensitive to properly track the vessel wall radial motion. As a result, brand new motion tracking methods had to be designed.

Accordingly, the final aims came to be:

1. *Study and refine the pre-existing, but yet unpublished, tracking method created by Cinthio M. for motion tracking in RF-data.*
2. *Record and beamform new in vivo ultrafast ultrasound recordings of the right common carotid artery.*
3. *Develop a brand new motion tracking algorithm for motion tracking on quadrature (IQ)-data of the new in vivo recordings.*
4. *Confirm the presence of an incident pulse wave in the new in vivo recordings by visually inspecting extracted motion data through Pulse Wave Imaging (PWI).*
5. *Further develop the tracking method in (3) to quantitatively estimate local PWV and determine both phase velocity and vascular impedance in the new in vivo recordings.*

6. *Potentially combine the developed method in (5) and its measurement results with flow data to determine vascular power.*

By determining the vascular power, this study would not only carry on the work of Eriksson A. and other department employees; but also put this in-house concept closer to clinical practice. Furthermore, this thesis project was supposed to be a confirmation and presentation to the world that vascular impedance and vascular power may be obtained through bare radial motion data of arteries collected non-invasively with ultrasound machines, without the need for simultaneous invasive pressure- and flow measurements.

The thesis project is expected to contribute to the creation of future tools for qualitative non-invasive estimations of cardiovascular systems health condition and other vascular mechanisms. The resulting measurements would thus be an indirect version of today's blood pressure measurements, but with less error sources. When refined, future clinical personnel are supposed to use this tool to indicate the presence of cardiovascular disease at an early stage and, thus, enabling earlier treatments than today.

1.3 Previous results and interest outside of the department

Great consideration has been taken throughout this thesis project in relation to the previously performed work and the projects historical background at the department.

Through *in vitro* experiments, by using simulated blood flow through tubular flow phantoms, Eriksson *et al.* showed that vascular impedance can be non-invasively measured to an absolute level by estimating phase velocity from PWV-measurements [2].

Extraction of vascular impedance data from such a measurement is shown in **Figure 1.3** – **Figure 1.4** together with reference impedance data calculated from simultaneous invasive high-fidelity pressure and flow measurements in **Figure 1.2**.

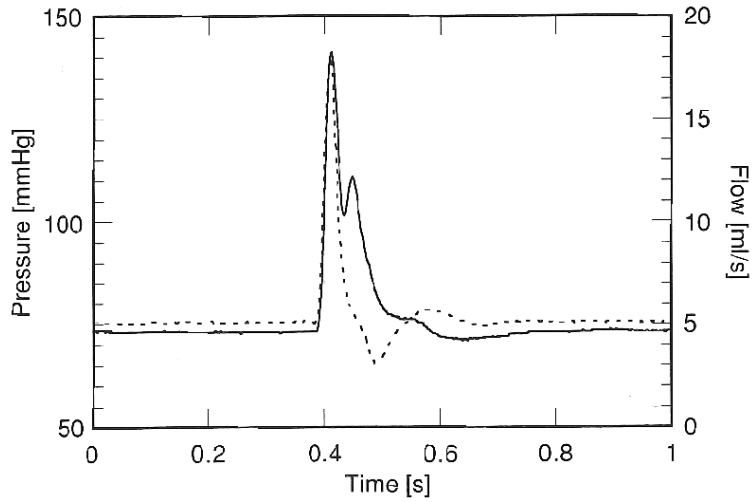


Figure 1.2: Examples of pressure- (—) and flow (---) recordings used to estimate the reference in **Figure 1.4**. Performed by Eriksson et al. [2]. Used with permission from Eriksson A. [2].

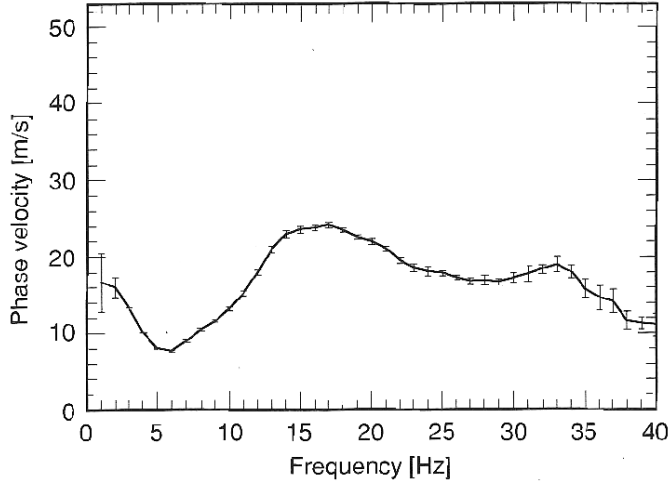


Figure 1.3: Example of phase velocity profile determined from membrane pulsations, $\pm 1SD$. Performed by Eriksson et al. [2]. Used with permission from Eriksson A. [2].

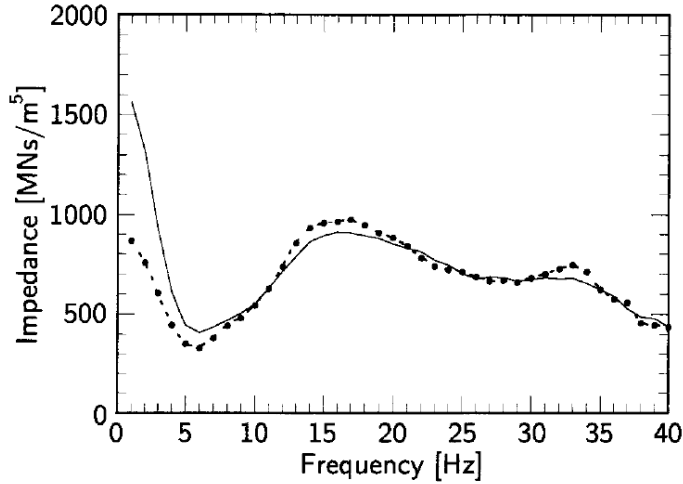


Figure 1.4: Example of estimated vascular impedance from the phase velocity (\cdots) compared to the reference ($-$). Performed by Eriksson et al. [2]. Used with permission from Eriksson A. [2].

The department has had, and still have, active cooperation with a number of departments within the medical faculty with large interest in this field. Such examples of collaborators are professor emeritus Karel Marsal at the Department of Obstetrics and Gynaecology, Lund University, professor Per Wollmer and doctor Åsa Ryden-Ahlgren at the Department of Clinical Physiology, SUS Malmö and the now late professor Toste Länne at the Department of Vascular Surgery, Linköping University.

2. Theory

2.1 Ultrasound

Ultrasound is like regular sound a mechanical vibration within a medium. The frequency of ultrasound is, however, above the human audible range of 20 kHz [2]. It has a diverse range of application, but is surely most commonly encountered by the public as medical ultrasound. In medical applications, ultrasound is usually operated at frequencies between $2\text{-}15\text{ MHz}$ [4].

The ultrasound is most commonly produced by utilizing piezoelectric elements, mono- or polycrystalline materials that either expand or contract when subjected to positive or negative electrical voltage respectively. In a similar manner, the material also generates electrical voltage when compressed or stretched. This property is known as the piezoelectric effect, which is effectively utilized in ultrasound technology today. In medical ultrasound, piezoelectric elements are usually fitted close together in transducers that either separately or simultaneously transmit and/or receive ultrasonic pulses.

The ultrasound waves generated into a medium can be of either longitudinal- or transversal nature and have their own regions of application. In many cases, including traditional ultrasound imaging, longitudinal waves are of higher relevance. The speed of sound inside a medium (v) of a longitudinal wave is related to the properties within the medium as much as it is to properties of the ultrasound itself. In relation to the medium properties, the medium's speed of sound is given by:

$$v = \sqrt{k/\rho} \quad (2.1.1)$$

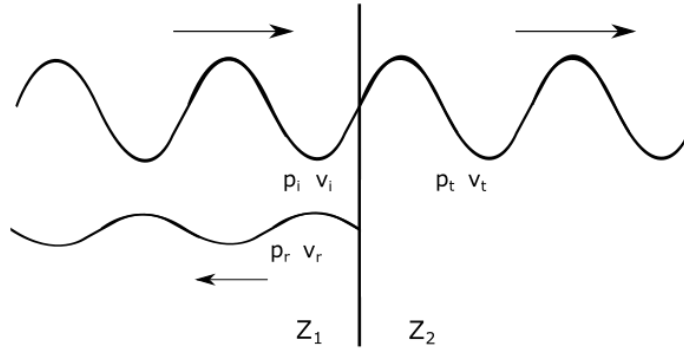
where k is the medium stiffness and ρ is the medium density. The ultrasounds wavelength (λ) is related to the ultrasounds frequency (f) and the mediums speed of sound in the following manner:

$$\lambda = \frac{v}{f} \quad (2.1.2)$$

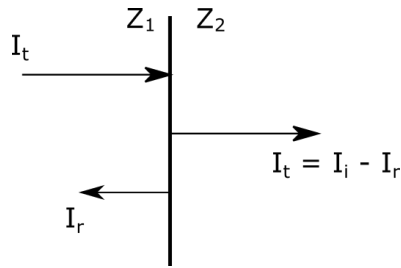
Because of its high frequency, ultrasound in transmission has a narrow radiation pattern as a narrow beam. Through this property, it is possible to point the ultrasound in a certain direction [2]. When the ultrasound is transmitted through a medium, it is subjected to both attenuation and reflection. Apart from reflection and attenuation, the ultrasound may also be influenced by scattering and refraction. The reflections, echoes, are produced when the ultrasonic wave travels through a homogenous part of a medium and reaches a boundary with another medium. At each medium interface the ultrasound reaches, some of its energy will be reflected to some degree while the rest continues into the next medium. The degree of reflection at each medium interface is determined by the difference in wave velocity and density of the two materials known as the difference in acoustic impedance between the two media. The acoustic impedance ($Z_{acoustic}$) is the resistance to pressure which the ultrasound experiences when traveling through the medium and is defined as:

$$Z_{acoustic} = \rho \cdot v \quad (2.1.3)$$

An illustration of ultrasound behaviour at one such medium interface is shown in **Figure 2.1** below.



(a) Ultrasound transmission and reflection in relation to pressure.



(b) Ultrasound transmission and reflection in relation to intensity.

Figure 2.1: Transmission and reflection of an incident ultrasonic wave at a medium interface, both in sense of pressure amplitude (a) and intensity (b). Inspiration from Hoskins et al. [5].

The ratio of reflections at a medium interface is expressible both in terms of pressure and intensity of the ultrasound waves. The amplitude reflection coefficient, R_A , is derived from:

$$R_A = \frac{P_r}{P_i} = \frac{Z_2 - Z_1}{Z_2 + Z_1} \quad (2.1.4)$$

where P_r and P_i are the pressure amplitudes of the reflected and incident waves respectively, whereas Z_1 and Z_2 are the acoustic impedances in the first and second mediums respectively. The intensity reflection coefficient, R_I , is defined as:

$$R_I = \frac{I_r}{I_i} = R_A^2 = \left(\frac{Z_2 - Z_1}{Z_2 + Z_1} \right)^2 \quad (2.1.5)$$

where I_r and I_i are the intensities of the reflected and incident waves respectively. The total wave pressure and velocity at the interface in medium 1, that is those of the incident and reflected waves, must be equal to that of the transmitted wave close to the interface in medium 2, i.e. $P_i + P_r = P_t$ and $v_i + v_r = v_t$ [5]. Other factors, such as the angle of incidence, the width of the medium structure and the angle of the medium interface play part in how many reflections return back to the transducer [4].

By recording the echoes returning to the transducer, an image is formed. The ultrasound image may be represented in a variety of ways. In medical ultrasound, the ultrasound image is often given as a 2-D image known as a B-mode image. It is, however, also possible to present the ultrasound image in 1-D, 3-D or 4-D (3-D + time). A B-mode (brightness mode) image is a two dimensional slice of the object being investigated. It is composed out of an adjacent series of vertically oriented scanlines, running from top to bottom where each scanline represents a series of piezoelectric element used for recording returning echoes. The pixels within the image are assigned a specific shade based on the amplitude of the returning echoes from black to white. The stronger the echo, the lighter the shade. The vertical position of each pixel/echo is derived from the echoes time of travel and the speed of sound, where the latter is assumed to be constant [3].

The process of determining the distance to distant objects by listening for echoes from transmitted ultrasonic pulses is referred to as the pulse-echo technique. In the wild, it has been used by animals like bats and toothed whales for navigation and localization of food sources for tens of millions of years. Humans, in comparison, started utilizing ultrasound through advances of electronics during the start of the twentieth century, where one application was to record the depth below ships. Today, ultrasound has a wide and diverse area of application such as non-destructive material testing, flow measurements, cleaning, pattern recognition and medical applications. The usage of ultrasound for medical applications started during the early 1950's where John J. Wild *et al.* were the first to detect tissue layers, George D. Ludwig and Francis Struthers *et al.* tried to localize gall stones and Inge Edler (AD 1911-2001) and Hellmuth Hertz (AD 1920-1990) pioneered the use of ultrasound to study heart movement, echocardiography. Ultrasound scanners that produce real-time images were first commercially available during the mid-1970's. Ultrasound is today one of the most dominating imaging systems in clinical practice [2].

Ultrasound data may be signal processed in several ways. The B-mode image is represented as either raw data directly or through the envelope of the signal processed raw data. RF-data is the raw, unprocessed, data from the ultrasound machine. It includes the transducer pulse frequency, the centre frequency, which must be removed to prevent ripple artefacts. There are two signal processing techniques commonly used in the field of ultrasound image representation: quadrature detection and Hilbert transformation [6].

Quadrature detection, IQ-data, is a demodulation where the raw data is mixed by after having been multiplied with a cosine- and sine-function with the same centre frequency as the RF-data. Both parts are then low-pass filtered, becoming I- and Q-data respectively. A concept illustration of the creation of in-phase and quadrature components, i.e. the I- and Q-data, is given in **Figure 2.2** below.

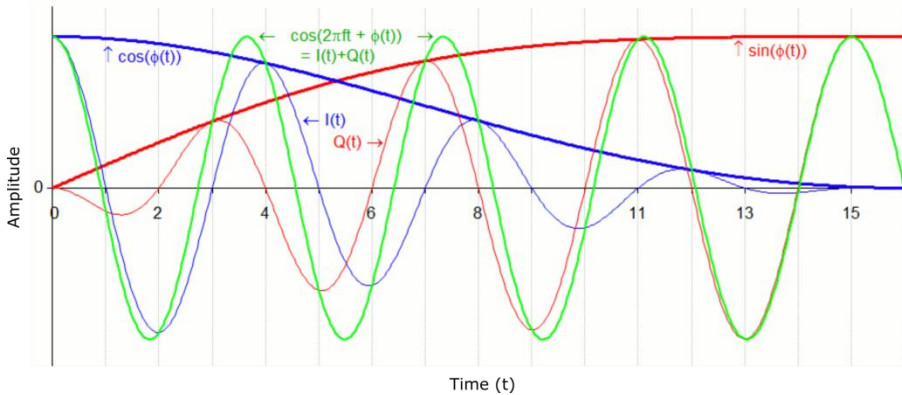


Figure 2.2: Concept of carrier signal (green, thin) and the formation of in-phase- (blue, thin) and quadrature signal (red, thin). The envelope of the in-phase- (red, thick) and quadrature signals (blue, thick) are also illustrated.

In **Figure 2.2**, the carrier signals phase angle is increased through non-linear modulation from 0 to $\pi/2$ over the interval $0 < t < 16$. The modulated signals, i.e. the I- and Q-signals, are offset in phase by $\pi/2$ radians but have the same nominal frequency as the carrier signal. In ultrasound context, the final B-mode image is retrieved by extracting the envelope through the mixed signals absolute value. This signal processing technique reduces effects created by out-of-bounce noise, but is associated with some blurring [6].

The Hilbert transform is created by nulling the negative frequencies in the Fast Fourier Transform (FFT) of the RF-data. The signal is then reconstructed back into the time-domain through Inverse Fast Fourier Transform (iFFT). The result is a 90° ($= \pi/2$ radians) phase shift of the original RF-data, now representing the Q-data. The I-data, on the other hand, is represented by the original RF-data. Lastly, by extracting the absolute of value of the combined signals, the B-mode image is retrieved. This signal processing technique has become popular through the technological development of increasing sample rates and higher digital processing capabilities. The Hilbert envelope gives a good approximation of the ultrasound pulse energy, but it also reduces

ripple artefacts in the B-mode image as well as it maximizes image detail. To faithfully calculate the Hilbert transform is, however, computationally costly. Nonetheless, it is possible to overcome this hurdle by either limiting the effective frequency range or by reducing the faithfulness computations. This gives a reduced, but in many cases acceptable, image quality in the final B-mode image [6]. An illustration is given in **Figure 2.3**.

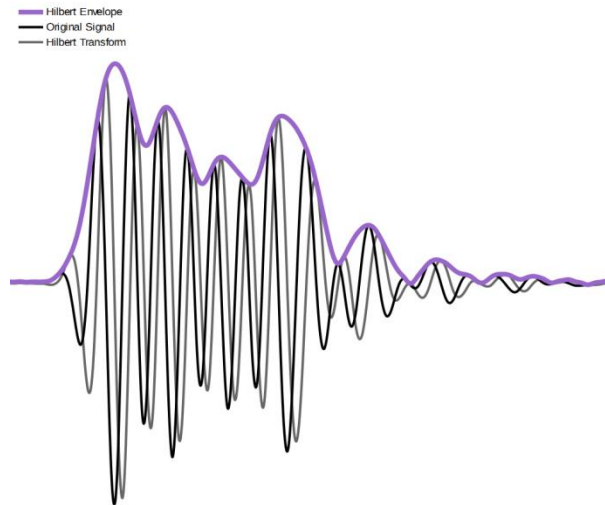


Figure 2.3: RF-signal, Hilbert transform and Hilbert envelope. IQ envelope. Used with permission from Starfish Medical [6].

An example of an *in vivo* B-mode image of the right common carotid artery is seen in **Figure 2.4** below. In ultrasound images like **Figure 2.4**, the outer- and innermost layers of the artery, the intima and the adventitia, are clearly visible. The middle layer of the artery however, the media, is shown as the dark band in between the intima and adventitia echoes. The proximal- (closest to the heart) and distal parts (closest to the brain) of the artery are shown to the right and left respectively in the image.

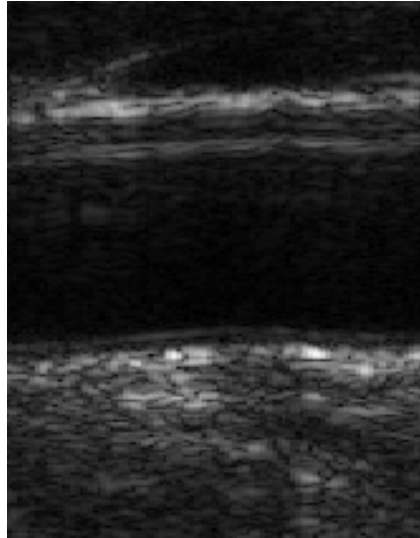


Figure 2.4: Example of in vivo recording of the right common carotid artery.

2.2 Ultrasound imaging techniques

Ultrasound is a non-ionic imaging technology that utilizes returning echoes of transmitted ultrasonic pulses to produce its images. Depending on how the ultrasonic pulses are transmitted, the imaging techniques will have different properties and potential uses. Two imaging techniques are frequently in use today: focused imaging and pulse wave imaging.

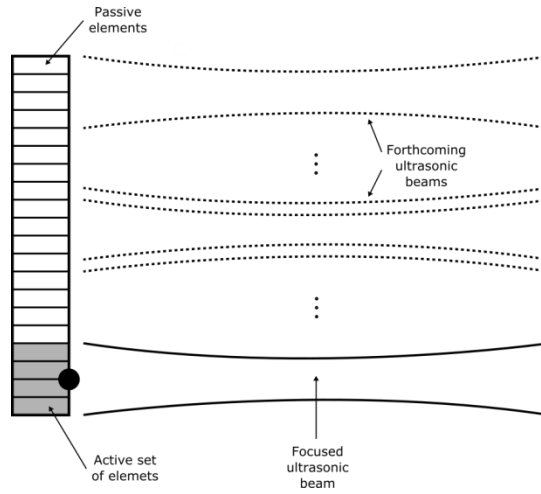
Focused imaging, also commonly referred to as conventional imaging, is formed by activating a set of piezoelectric elements, a scanline, within the transducer. This focuses the ultrasonic waves and forms a beam, known as the transmission beam. During this procedure, all other elements remain passive. After transmission, the transducer goes into reception mode where the piezoelectric elements are passive, listening for the returning echoes. The number of active elements in

reception is initially small, e.g. one or two elements, forming another focused ultrasonic beam; the reception beam. By progressively increasing the number of listening elements, the reception beams focus point is progressively moved deeper into the medium. This creates a progressively focused beam for the returning echoes, known as a focused reception beam. After completion, the transmission/reception procedure is begun anew by moving the scanline a certain distance, e.g. one element width. A B-mode image created through focused imaging is thus updated in a sweeping manner, one scanline at a time. This technique is associated with great focus in both transmission and reception, but also suffers from lower frame rates. Since the transmission- and reception procedure is repeated for every scanline, where only one scanline is active at a time, the frame rate is limited to up to 100 Hz [7].

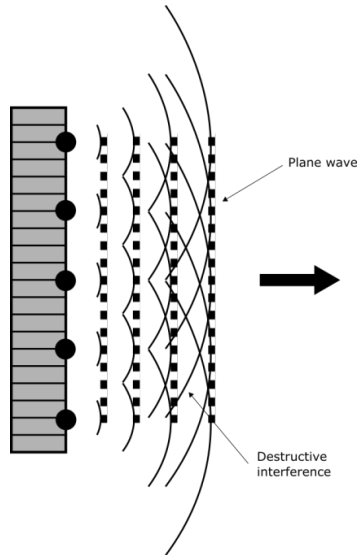
Plane wave imaging is an ultrasound imaging technique that is utilized to record fast events within a medium. By activating all piezoelectric elements in groups at once, constructive- and destructive wave interferences form a plane, forward propagating, pulse wave; hence its name. By this approach, the frame rate is drastically increased. In ultrafast plane wave imaging, frame rates up to 20 kHz have successfully been applied. The number of active scanlines is, however, fairly limited; commonly spanning a few tens of scanlines (64-512) [7, 8].

By utilizing the same basic principles as in plane wave imaging, but by activating the scanlines subsequently, the plane wave may be steered. The angle is determined by the time in between activations of each scanline. If consecutively taken with plane waves in different angles, frames may be combined to improve image quality by reducing speckle and other acoustic artefacts. This technique is called compound imaging [9].

A graphical illustration of both focused- and pulse wave imaging in transmission is found in **Figure 2.5** below.



(a) *Focused imaging in transmission. Once finished in reception, the scanline is progressed by one piezoelectric element.*



(b) *Plane wave imaging in transmission.*

Figure 2.5: *Focused- and plane wave imaging techniques in transmission. In both (a) and (b), each scanline comprises of four piezoelectric elements. Inspiration from Hoskins et al. [5].*

2.3 The circulatory system and its historical background

The practice of pulse interpretation for diagnostic purposes is traceable back to approximately 4000 years ago. According to legend, the technique of feeling the pulse, sphygmology (from the Greek word sphygmos: pulse), was founded by the Chinese emperor Hoamti in 2500 BC. Sphygmology was considered as much a science as an art form for physicians to perform and master. The pulse of the patient would be timed against the respiration of the physician, where four pulses per respiration was considered as normal for adults. The palpation was performed by using the index, ring and middle fingers at three different locations along the wrist. At each location, light, middle and firm pressures would have been applied to feel the superficial and deep pulses. The whole procedure would have taken several hours and the pulse would later be described by using different metaphors such as “the jump of a frog”, “the tail of a fish” or “raindrops falling on the roof” [2].

The overall idea in sphygmology was that each organ had its own characteristic pulse and if a particular pulse would be found in the wrong place, a serious disorder in the system would have been indicated. To further complicate the situation, different organs would have dominated others on a seasonal basis. As an example, in spring the pulse of the liver would normally be dominating; whereas to have the pulse of the lung dominating at this time would have been seen as a mortal sign. Some organs, however, were said to be related to each other. To have the pulse of the heart in spring would have been considered less serious, this since the heart was seen as the son of the liver. In total, 16 different mortal pulses would have indicated death within a time span between 24 hours and 5 years. In comparison with modern medicine, the anamnesis (the case history of the patient) was not considered as important. Instead; the symptoms, the organs affected

and the prognosis were solely said to determine the illness based on the pulse [2].

Over the course of history, sphygmology were to be highly developed in other cultures as well; especially by the Hindi and ancient Greek civilizations. The Hindu physicians in particular showed many similarities with their Chinese counterparts, despite being separated by nearly 2000 years. The Hindus thought it central for both the patient and physician to be at ease during the examination. As in China, metaphors were used to describe the pulse. Here, the descriptions were also inspired by animal motion as e.g. serpents, frogs, swans and peacocks. But in contrast to the Chinese, Hindus only palpated one wrist; the right in men and the left in women. They also deviated from the Chinese by not believing the deviations from the normal pulse to be associated with different organs, but rather to an imbalance between the three humours air, phlegm and bile [2].

It was during the ancient Greek civilization that sphygmology reached its golden age, especially through the Greek Claudius Galenus (AD 131-200). Galenus is by many considered the foremost sphygmologist of the ancient world, indeed of all time. He was an active teacher in the field and wrote more books on sphygmology than anyone else; whose ideas would dominate clinical practice for more than 1600 years. The pulse was, in his opinion, defined by a dual movement pattern of the artery being expanded and contracted, today known as diastole and systole respectively. Diastole was considered an active expansion that attracted the blood from the heart, while systole more of a passive phase. He also recognized the arterial pulse to be dependent of and synchronous with the heart. Similar to the Chinese, Galenus believed in organic pulses and researched extensively how the pulse was affected by various parameters like age, season, food and wine, sleep and exercise. Galenus thought the cardiovascular system to be a one-way system where the blood, after being produced by the liver by nutrients, was transported to the right side of the heart. Inside the heart, the blood

would be separated into two parts: one for the lungs and the other being diffused through the septum to the left side of the heart. While in the left side of the heart, the blood would be mixed with air to create the so called “life spirit” which was later transported out to the peripheral body and absorbed [2]. Another important publication in the field of sphygmology was published in 1540, *Ars Sphygmica* by Professor Joseph Struthius (AD 1510-1568). Within it, Struthius gave the first ever description on how to visualize the pulse. This was done by placing a leaf on top of the artery to observe the vibrations generated by the passing pulse. His greatest achievement was, however, that he systemized the field of sphygmology [2].

It would not be until the seventeenth century that Galenus ideas were to be challenged by the man William Harvey (AD 1578-1657), today considered the discoverer of the circulatory system. His ideas were, however, not new at the time. Harvey’s true contribution came in the extensive and precise argumentation of his *Expericitatio anatomica de motu cordis et sanguinis in animalibus* (Anatomic thesis on motion of the heart and blood in animals), which was published in 1628 and contained evidence based on logic lines of arguments and a series of experiments on both humans and animals. In his thesis, Harvey argued the hearts contraction phase to be the active phase and expansion as the passive by conducting a vivisection. The animal’s heart being observed became stiff during contraction and later flaccid after expansion. In addition, he claimed the pulsatile dilatation of the arteries to be a result of the heart’s pumping action. This was quite different from the general view at that time, being that blood reached the peripheral parts by active vessel expansion. He also stated that the blood was circulating and ended up describing the circulatory system in detail, claiming the blood to be pumped from the left ventricle, through the arterial system and brought back to the right atrium by the venous system. In his thesis, Harvey made three assumptions:

- The amount of blood pumped from the heart exceeds by far the amount of consumed nutritive.
- Based on the cardiac output, the available blood volume would have passed the heart after a short period of time.
- Blood is continuously brought back to the heart by the veins.

The first two assumptions were proved by simple calculations on heart rate stroke volume, while the third was assessed through an experiment where blood flow was stanced in the forearm by applying a tight bandage pressing the superficial veins, blood could be seen being transported back to the heart while the vein valves prevented any backflow. The one thing Harvey did not fully understand was the transition of blood from the arterial to the venous side. This would later be revealed when Marcello Malpighi (AD 1628-1694) discovered the capillary system in 1661 [2].

As we know today, the circulatory system consists of a series of interconnected vessels in a complex manner. Oxygenated blood emerges as a flow from the hearts left ventricle to the aorta. On its journey to the peripheral system, the blood continuous by passing through the main arterial branches, terminal arteries, arterioles and finally the capillaries. The individual vessels cross-sectional area changes drastically with ever decreasing diameter as the system progresses; from the dimension of centimetres in the aorta and arteries to the diameter of blood cells within the capillaries. Thanks to the vascular systems highly branched structure, every metabolically active cell is assured a sufficient supply of nutrients since every cell within the capillary network is less than 100 μm away from a capillary [10].

In **Figure 2.6** is a graphical representation displayed of the systemic blood pressure appearance in various parts of the circulatory system. Systemic blood flow, in a similar manner, do also vary within the circulatory system, leading the pressure. Once the arterioles are reached, both pressure and flow drastically decreases and changes from pulsatile pressure and flow into almost constant in the capillaries and the venous side of the circulatory system.

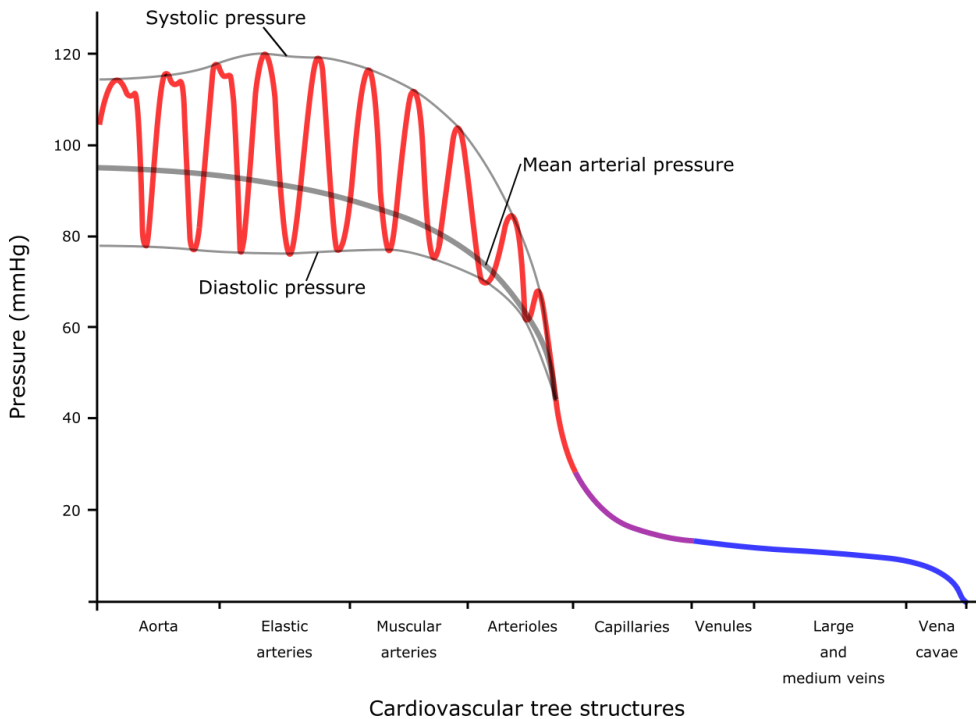


Figure 2.6: Systemic blood pressure. The graph shows the components of blood pressure in vessels throughout the body, including systolic, diastolic, mean arterial and pulse pressure. Inspiration from Lumen Learning [11].

Even after Harvey had published his *Expericatio anatomica de motu cordis et sanguinis in animalibus* in 1628, several publications on sphygmology continued to appear for several centuries. It would not be until the publication of *The Study of The Pulse* in 1902 by James Mack-

enzie (AD 1853-1925) that sphygmology ceased to exist in clinical medicine [2].

Surprisingly enough, objective measurements of the human pulse were made relatively late in regard to its long historical use. Among the first known instruments designed to time the pulse was the pulsilogon, created by Galileo Galilei (AD 1564-1642) in the late sixteenth century. The pulsilogon consisted of a lead bullet pendulum tied to a graduated silk string. By adjusting the length of the string, the pendulum's motion was synchronized to the pulse. The pulse rate could then be read from the graduated marks on the string [2]. In 1733, the first blood pressure measurements were performed on a horse by Stephen Hales (AD 1677-1761) by observing the increase and decrease in pressure as blood moved up and down a long glass tube inserted into one of the horse's arteries. The first sphygmomanometer, also known as a blood pressure meter, was created in 1881 by Samuel Siegfried Karl Ritter von Basch (AD 1837-1905). Blood flow was restricted by a water filled rubber bulb connected to a mercury column, from which the pulse was read in units of millimetres of mercury, *mmHg*. The sphygmomanometer would later be improved by applying a cuff on the limb of interest to deliver even pressure, which was done by Scipione Riva-Rocci (AD 1863-1937) in 1896. Still used to this day, modern procedures of blood pressure measurements were developed in 1905 by Nikolai Korotkoff (AD 1874-1920) from his discovery of the difference between systolic- and diastolic blood pressure [12]. During the twentieth century, due to rapid development in sensor technology, several new tools for detailed hemodynamic analysis were developed. Pulsatile pressure was, however, studied much earlier than pulsatile flow since the technological requirements needed for manometers was simpler than that of flowmeters. Otto Frank (AD 1889-1980) did pioneering work on manometers at the start of the twentieth century. Catheter tipped pressure transducers were firstly introduced in the mid-1940's and had, compared with the previously existing fluid filled systems, an extended bandwidth. It would, however, not be until the

mid-1960's until they were practically usable; one of which were the first sensors to be used to monitor pulsatile blood flow. Ultrasonic flow probes were introduced at the start of the 1960's, utilizing either transit time- or Doppler technology. Transit-time probes estimate the spatial average flow velocity, while pulsed Doppler probes can record the flow velocity profile. It would not until the 1980's that multi-sensor catheters became commercially available, allowing for multiple pressure- or combined pressure and flow recordings to be performed.

2.4 The arterial wall and its properties

Arteries are the vessels responsible for carrying oxygenated blood from the heart to the capillaries of the peripheral body structure. They may be split into three categories depending on their characteristics: elastic arteries, muscular arteries and arterioles. They do, however, still have a similar structural composition composed of three concentric regions: the intima, media and adventitia. An illustration is given in *Figure 2.7* below [2].

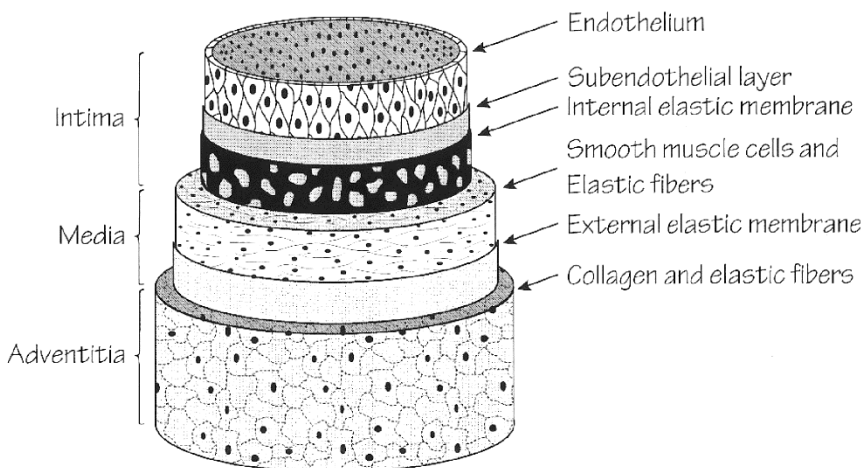


Figure 2.7: General composition of the arterial wall. Used with permission from Eriksson A. [2].

The intima works as an internal coating facing the lumen, i.e. the blood. It is composed out of three sublayers: the endothelium, the subendothelial layer and an internal elastic membrane [2]. The endothelium consists of a single layer of endothelial cells that control the vascular relaxation and contraction mechanisms, the clotting of blood, immune functions and platelet adhesion by releasing enzymes and other substances [13]. The subendothelial layer is a loose connective tissue layer that may contain smooth muscle cells, while the internal elastic membrane is a composition of elastic tissue fibres and works as a separating layer to the media [2].

The media is the largest region of the artery and determines its mechanical properties. It consists of a concentric layer of smooth muscles cells as well as elastin, shielded from the adventitia by an external elastic membrane. The amount of elastin in the media increases with the size of the artery [2].

The adventitia is a combination of longitudinally oriented collagen (type III) and elastic fibres, where the collagen contributes to the arteries tensile strength. The adventitia's outer layer is not well defined, but rather becomes gradually more integrated with the surrounding tissue. It is also in the adventitia of the larger arteries that the vasa vasorum, small supplying blood vessels of the media and adventitia, are found [2].

Elastic arteries, represented by the aorta and its large branches (the common carotid-, pulmonary- and subclavian arteries), are large and conductive vessels characterized by predominate composition of elastic fibres to muscle cells within their medial layer. These elastic fibres are oriented as concentric sheets and increase in number with age, leading to increased lamina thickness and a decrease in vessel elasticity. In new-borns, the media has approximately 40 sheets of elastic fibres while adults may have as many as 70 sheets [2].

Most named arteries within the body, apart from those named above, belong to the category of muscular arteries. They are medium sized and distributing vessels, ranging down to 0.5 mm in diameter, characterized by their predominate medial composition of smooth muscle cells over elastic fibres. The media in muscular arteries may contain as many as 40 layers of smooth muscle cells while their adventitia is, in relation to their media, relatively thick [2].

Arterioles are small and connective vessels, less than 0.1 mm in diameter, between muscular arteries and capillaries. Their medial layer content of smooth muscle cells does not exceed three layers and the number of elastic fibres is as good as negligible. The adventitia is also very thin and does not contain any elastic lamina [2].

The arterial wall is thus an inhomogeneous structure of several layers with different mechanical properties. These wall properties vary throughout the circulatory system by its composition and component architecture. But it is, independently of the relative position within the circulatory system, regarded as a “two phase” material meaning the elastin is load bearing during small vessel dilations while both collagen and elastin are combinedly load bearing during larger vessel dilations. This gives rise to a non-linear relationship between pressure and arterial wall diameter, illustrated in *Figure 2.8* below [2].

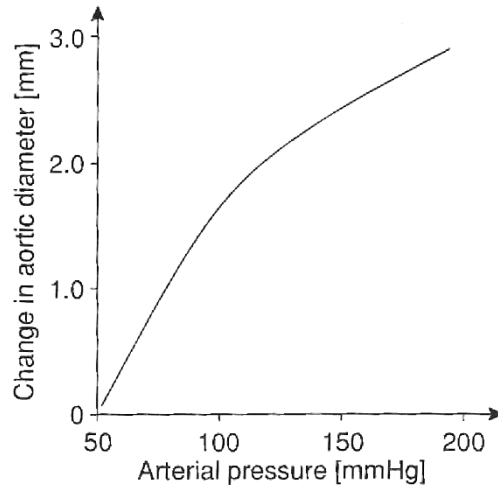


Figure 2.8: Pressure-diameter relationship in the abdominal aorta. Used with permission from Eriksson A. [2].

The arterial wall structure does, as mentioned above, change with increasing age; primarily in the intima and media layers. Within the intima do cells within the endothelial sublayer become irregular in shape and size as well as the subendothelial layer thickens. As for the media, its elastic fibres lose their original orientation and experiences splitting as well as fragmentation. The amount of collagenous fibres also increases, often with calcium rich deposition, resulting in increased arterial stiffness. The change is not only structural since their geometrical appearance is also altered, this in the way of increased arterial radius and wall thickening. As an example has an increase in internal diameter been reported for the ascending aorta in humans of 9 % per year between age 20 and 60 [2].

There are several parameters to characterize the mechanical properties of an artery as well as the cardiovascular system. None of them is, however, perfect. Some of these may even be estimated from non-invasive ultrasound measurements such as arterial strain, pressure stra-

in elastic modulus, pulse wave velocity (PWV) and vascular impedance. These parameters will be described to some extent below, while PWV and vascular impedance will be further investigated later on since they are key parameters to this thesis.

To recap from section 2.1, the speed of sound within a compressible medium, originally derived by Isaac Newton (AD 1643-1727), is defined by:

$$c = \sqrt{k/\rho} \quad (2.4.1)$$

where k is the stiffness and ρ the density of the material. This expression may be used in analogy of wave propagation in incompressible media within an elastic tube. In vessels and arteries, this is referred to as pulse wave velocity (PWV).

The material stiffness may also be referred to as the volume elasticity, and if it is expressed as:

$$k = V \frac{\partial P}{\partial V} \quad (2.4.2)$$

where P is the pressure and V the volume of the material, and the length of the vessel is assumed constant, the expression in equation (2.4.1) can be rewritten as:

$$c = \sqrt{V \frac{\partial P}{\rho \partial V}} = \sqrt{\frac{\pi r^2 \partial P}{\rho 2\pi r \partial r}} = \sqrt{\frac{r \partial P}{\rho 2 \partial r}} \quad (2.4.3)$$

where r is the radius of the vessel. Thus, for a given pulsatile pressure ∂P , the propagation velocity will increase as the vessels radial dilatation ∂R decreases with rising arterial stiffness. The propagation

velocity has also shown relationship with the Young's elastic modulus in the circumferential direction E by:

$$c = \sqrt{\frac{Eh}{2r\rho}} \quad (2.4.4)$$

where h is the vessel wall thickness. The equation (2.4.4) is also known as the Moens-Korteweg formula. However, this formulation has been proven practically limiting since the wall thickness is difficult to determine precisely *in vivo*.

More frequently used quantities are the pressure-strain elastic modulus (E_p) and the related arterial strain (ε) [2]. Arterial strain is defined as the extension of the vessel wall in relation to its original dimensions and has been shown to be related to arterial stiffness and other cardiovascular risk factors [14]. It is related to the vessel diameter during maximum systolic- and end diastolic pressure as:

$$\varepsilon = \frac{d_{systole} - d_{diastole}}{d_{diastole}} = \frac{\Delta d}{d_{diastole}} \quad (2.4.5)$$

where $d_{systole}$ and $d_{diastole}$ is the diameter during maximum systole- and end diastole respectively. The pressure-strain elastic modulus is derived from:

$$E_p = \frac{P_{systole} - P_{diastole}}{\varepsilon} = \frac{\Delta P}{\varepsilon} \quad (2.4.6)$$

where $P_{systole}$ and $P_{diastole}$ are the maximum systole- and end diastole pressures. Arterial stiffness is thus related to both blood pressure and arterial strain. The pressure strain elastic modulus has been shown to increase with age in humans, illustrated in **Figure 2.9** below [2].

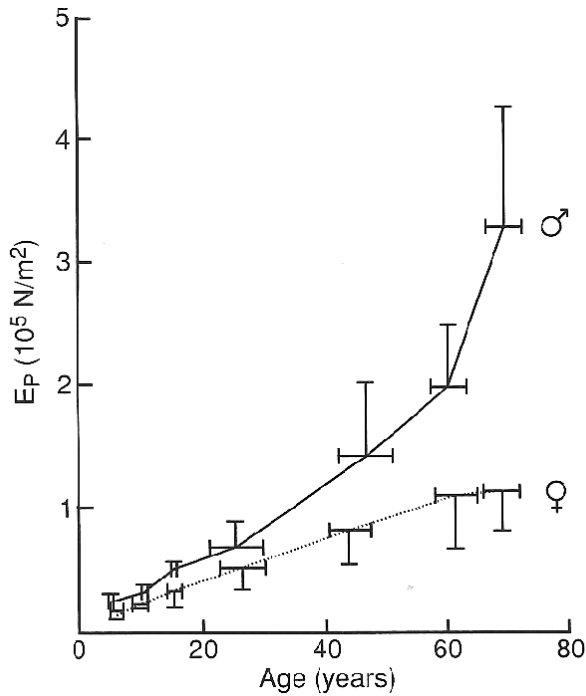


Figure 2.9: The pressure strain elastic modulus (E_p) in the human abdominal aorta. Used with permission from Eriksson A. [2].

As is shown, E_p tends to increase linearly in women and non-linearly in men. Through the non-linear behaviour of E_p due to the vessel diameter and blood pressure relationship, E_p may be considered an unsuitable parameter for higher pulse pressures. For these situations, incremental elastic modulus (E_{inc}) is preferred but leads to the need of catheterization instead of simpler cuff-based pressure measurements [2].

Impedance may, generally speaking, be described as the opposition to flow presented to a driving force within a system. This terminology is used in multiple scientific fields such as electricity, acoustics, mechanics and, in this case, vascular circulation. In vascular circulation theory, the so called vascular impedance is the measurement of

hindrance to blood flow experienced by the heart [2]. By some, it has been referred to as “*the central problem in hemodynamics*” [15].

Originally introduced in 1955, it expresses the relationship between pulsatile pressure and pulsatile flow at some location within the arterial tree. The impedance (Z) is a complex quantity determined by relating the corresponding frequency components of the pressure- and flow waves. It consists of a modulus ($|Z(f)|$) and a phase ($\phi(f)$). By transforming the pulsatile pressure- (P) and flow data (Q) into the frequency domain, two sets of amplitude- and phase spectra are produced: $|P|$ and $\arg(P)$ for pressure; $|Q|$ and $\arg(Q)$ for flow. The modulus is defined by the quotient of the amplitudes:

$$|Z(f)| = \frac{|P(f)|}{|Q(f)|} \quad (2.4.7)$$

whereas the phase $\phi(f)$ is determined by the difference in phase:

$$\phi(f) = \arg P(f) - \arg Q(f) \quad (2.4.8)$$

In other words, the phase expresses the delay between pressure and flow waves. An illustration of the determination and graphical representation of the vascular impedance is found in **Figure 2.10** below [2].

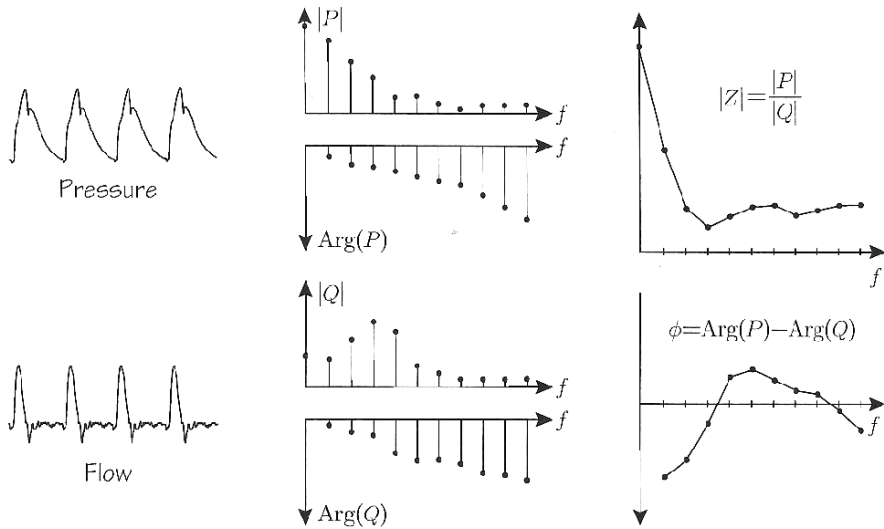


Figure 2.10: Procedure for determination and typical graphical representation of vascular impedance. Used with permission from Eriksson A. [2].

Because of its ability to locally characterize and describe the vascular bed below the measurement point, vascular impedance is of considerable importance in cardiovascular research. The whole arterial system, as an example, is reflected in the vascular impedance of the ascending aorta which hence describes the heart load seen by the left ventricle [2].

2.5 Pulse wave velocity

As the name implies, PWV expresses how fast the pulse wave propagates through the circulatory system. It is in some sense a highly local parameter since it may change from one place to another within the arterial tree system. It may also be regarded as a more global parameter by recording the arrival time and travel distance of the pressure wave at distal parts of the body, such as the upper limb and the leg. The upper limb is defined as the region in vertebrate animals extending from the deltoid region and includes the hand, arm, armpit and shoulder.

PWV increases gradually with age since childhood, independently of increased mean pressure. The increase has, however, been shown to be greater in populations more prone to hypertension than in other low risk groups. The increase in PWV is also known to be greater in the aorta than in any of the peripheral arteries, where it may more than double between the age of 20 and 80 in human test subjects. The growth rate of the aortic PWV (aPWV) with age have been found to be even higher during some monitory studies, from 4 *m/s* at age 25 to around 8 *m/s* at age 50 and 10 *m/s* in the late sixties; corresponding to a 150 % increase over 40 years. This makes it the greatest changing vascular parameter with aging apart from characteristic impedance (to be later defined). The increase in PWV is consistent with greater disorganisation of the arterial media layers in central elastic arteries, caused by fatigue and fracturing of the elastin fibres from increased pulsatile strain. In arteries of the upper limb, PWV only increase with age to a small extent. The PWV is thus a highly variable parameter depending on where in the arterial system it is measured and the age of the test subject. Since the PWV in the aorta is of particular interest, the use of some generalized transfer function is justifiable to non-invasively estimate the central aortic pressure wave from a radial artery pressure wave in adult humans. However, in relation to the ascending

aortic impedance modulus, increased PWV will more likely affect its low-frequency components more than the high-frequency components. This is due to a direct relationship between increased aortic PWV and increased aortic stiffness. In a similar manner, increasing aortic PWV is indirectly related to prematurely returning wave reflections. It has been shown that a two-fold increase in PWV is translatable to a four-fold increase in impedance modulus at low-frequency [16].

Studies of the change in PWV with age in humans have shown that central elastic arteries are initially, in infancy and adolescence, more distensible than the peripheral arteries. In other words, PWV is originally higher in the peripheral arteries than in the central elastic arteries. As time goes by, these elastic non-uniformities change and ultimately lost as the aorta progressively stiffens; making aPWV approach and potentially even exceed those of the peripheral arteries in test subjects over 60 years of age. However, this wave velocity was not measured in the most proximal parts of the aorta, so these data are not totally conclusive [16].

Apart from human circulatory arteries, the same non-uniformly elastic properties have been found in experimental animals as well. In studies regarding PWV and vascular impedance, it is especially common to compare measurement results from dogs with those of humans. This is due to dogs and humans having similar vascular properties and dimensioning of the arterial tree structure. A major difference between dogs and humans is, however, the lifespan. However, when expressing the progressive increasing PWV in terms of years, the change have been found surprisingly similar in both humans and dogs at around 4 % per year. And in the brachiocephalic artery of dogs, PWV has been found to increase with about 24 % over ten years. The degeneration of the elastic fibres within the human arterial wall is the most likely culprit behind increasing aPWV with age in humans as well as the inequality in impedance patterns, pressure- and flow wave contours between humans and animals [16].

The arterial dispensability also change as a consequence of aging, which has frequently been assessed from PWV measurements in the limbs, especially the upper limb. These measurements have been prone to underestimating the changes within the aorta however. Thus, findings within arteries of the limbs may not be directly extrapolated to properties of the central elastic arteries or the arterial system as a whole [16].

The progressive increase in PWV within arteries has also been confirmed by other measurements of arterial stiffness in human arteries. These measurements agree with the proposition that central arteries, predominantly the elastic arteries, experiences increasing PWV with age while peripheral arteries show little or no increase [16].

2.6 Wave reflections

Within the arterial system, there will be reflections of the pressure- and flow waves when an abrupt change in vascular impedance is eminent. This may be from naturally occurring sources as well as abnormal conditions within the vessel. They are typically present at stenosis, local stiffening of the vessel wall, bifurcations or in the transition between arteries and arterioles where their amplitude is determined by the degree of impedance mismatch [2].

Pressure- and flow waves are differently affected by reflections. Reflected pressure waves are added to the incident pressure wave, whereas reflected flow waves are instead subtracted from the incident flow wave. Consequently, ventricular load may be increased due to reflected pressure waves if they return during systole. For reflected flow waves, the effect is instead a decrease in cardiac output. The circulatory system thus works most efficiently when low amounts of wave reflections are present in the arterial tree structure [2]. The interactions between incident pressure- and flow waves and their

reflections are illustrated in *Figure 2.11*.

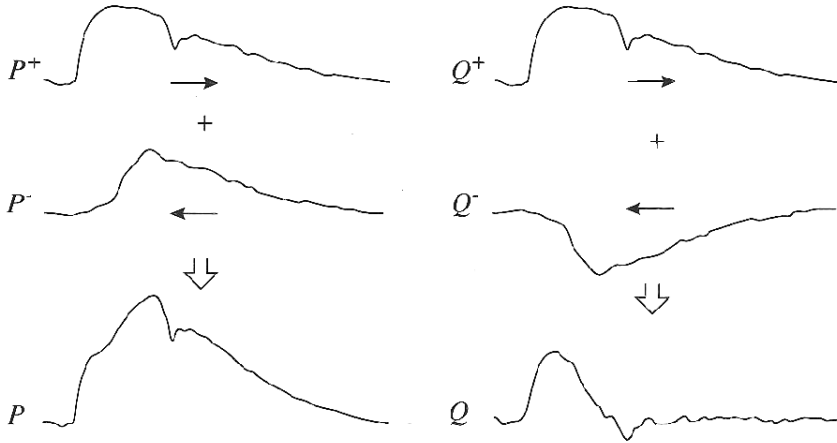


Figure 2.11: Human descending aortic pressure- and flow waves. The observed waves (P and Q) consist of the cardiac output (P^+ and Q^+) and the reflected waves (P^- and Q^-). Used with permission by Eriksson A. [2].

Wave reflections may thus arise from any discontinuity in the arterial tree; being it the trees dimensionality or elasticity. There are, however, some sites within the arterial tree structure where wave reflections are more noticeable than others; one of these sights being the common carotid artery. Opinions on the location of the major reflection site within the body, however, differ. Some argue the transition between arteries and arterioles as the major reflection site due to them having the largest impedance mismatch within the body. The human circulation would thus be able to be represented as an asymmetric T-tube where reflections are summed in two locations, one representing the upper body and the other the lower body. Others have proposed the major reflection site being located at the terminal aortic bifurcation or the aortic level of the renal artery branches instead, either alone or in combination with each other [2].

2.7 Vascular impedance

2.7.1 Terminology

The term impedance is, as was mentioned in section 2.4, a widely used concept in many scientific fields. As a result, it is a good idea to compare them with each other to get a better understanding of the terminology. As an example, vascular and electrical analogies of impedance are compared as follows.

Since the impedance is a complex quantity, composed out of a modulus and phase, it may be rewritten as:

$$Z = R + jX \quad (2.7.1)$$

where R and X is the resistive (resistance) and reactive parts (reactance) respectively. The resistance is mainly determined by the vessels cross-sectional area, where a flow resistance may be regarded as a simple obstruction. The reactance may either be positive (inductance) or negative (capacitance) in value. The inductance is a result of the blood mass movement inside the vessel, referred to as the fluid inertance or fluid inertia. The capacitance, on the other hand, is a result of the vessel wall elasticity, also referred to as vessel compliance. A visual comparison between these impedance analogies and their components is given in *Figure 2.12* below [2].

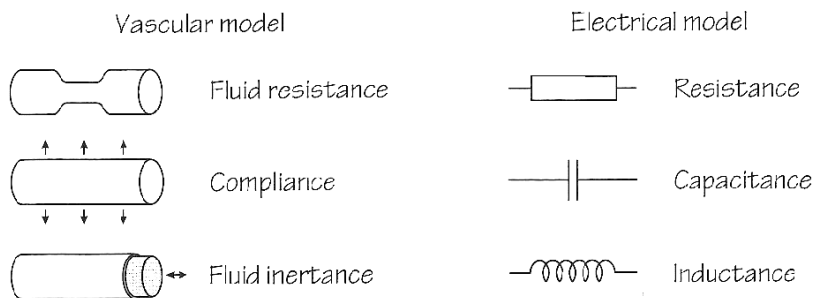


Figure 2.12: Impedance component analogies in vascular and electrical models. Used with permission from Eriksson A. [2].

Pressure (P) and flow (Q) in a vascular system may thus, in a similar manner, be directly translated into voltage (V) and current (I) respectively in the electrical model:

$$Z_{electrical} = \frac{V}{I} \quad (2.7.2)$$

$$Z_{vascular} = \frac{P}{Q} \quad (2.7.3)$$

In electrical terms, inductance acts as a preserver of flow and capacitance as a preserver of voltage. In other words, they preserve energy in one way or another inside the system. With some modifications, this explanation is also compatible with the vascular case where fluid inertia acts to preserve the blood flow and vessel compliance acts as a pressure reservoir [2].

Viewing the arterial tree system as a lumped impedance is, however, problematic. This is due to the combination of low propagation velocity (PWV) and physiological frequency range within the circulatory system. It makes wave reflections a potential problem. Transmission line theory may successfully be incorporated to counter

these issues, which otherwise is used in electrical engineering and catheter design. The vessel is then seen as a large number of small interconnected impedance segments like in **Figure 2.13** [2].

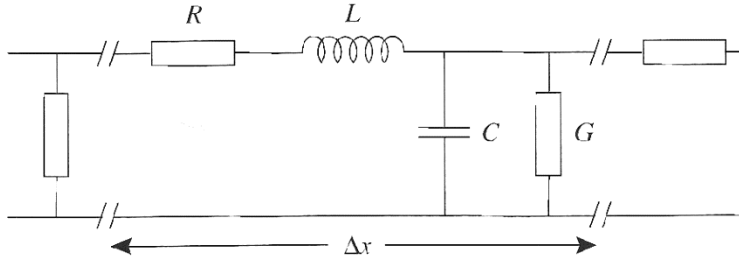


Figure 2.13: Concept of transmission line theory in vessel modelling. Used with permission from Eriksson A. [2].

Each segment consists of an inductance (L) and a capacitance (C) in parallel with each other representing fluid inertia and vessel compliance respectively. The losses within the segment are represented by a resistance (R) and a conductance (G). The unit of the impedance and its components are in “per unit length”. By letting the segment length Δx approach zero, a continuous model is created [2, 17].

In transmission line theory, transmission lines are characterized by two parameters: characteristic impedance, also known as surge impedance, (Z_0) and a propagation constant (γ). They are determined by:

$$Z_0 = \sqrt{\frac{R + j\omega L}{G + j\omega C}} \quad (2.7.4)$$

$$\gamma = \sqrt{(R + j\omega L)(G + j\omega C)} \quad (2.7.5)$$

where ω is the angular frequency given by:

$$\omega = 2\pi f \quad (2.7.6)$$

where f is the frequency of the signal present within the system [2, 17].

If the system would be regarded as lossless, i.e. $R = 0$ and $G = 0$, equation (2.7.4) and (2.7.5) may be rewritten as:

$$Z_0 = \sqrt{\frac{L}{C}} \quad (2.7.7)$$

$$\gamma = j\omega\sqrt{LC} \quad (2.7.8)$$

In a lossless case, characteristic impedance is real valued [2]. If L and C are given or known, it is possible to estimate the propagation velocity (PWV) within the segment by:

$$c = \frac{1}{\sqrt{LC}} \quad (2.7.9)$$

In cardiovascular theory, four versions of vascular impedances are commonly considered:

- Longitudinal impedance
- Input impedance
- Characteristic impedance
- Terminal impedance

Some sources also refer to an impedance term named transversal impedance. This impedance is used to characterize the compliance of an arterial segment that express the drop in flow at a given pressure due to energy storage in the vessel wall caused by the walls radial motion [18]. This impedance has, however, been left out of this thesis report.

2.7.2 Bringing vessel characteristics into an impedance model

In the circulatory system, there are three main contributors determining vascular impedance:

- The arterial tree geometry.
- The vessel walls elastic properties.
- The bloods hemodynamic properties.

The arterial tree geometry is affected by curvature, cross-sectional area and bifurcations in the arterial system. The cross-sectional area affects both fluid resistance R and inertia L , whose relations may be described as:

$$R = \frac{8l\mu}{\pi r^4} \quad (2.7.10)$$

$$L = \frac{\rho}{A} \quad (2.7.11)$$

where l is the length of the vessel, μ the fluid viscosity, r the radius of the vessel, ρ the fluid density and A the cross-sectional area of the vessel. Since fluid resistance is related to the vessel radius to the power of four, it is clear that smaller individual vessels, such as arterioles, exhibit considerably higher fluid resistance than larger vessels, such as the aorta [2].

The fluid resistance is also increased if the vessel is curved. This influence is quantified by using the Dean number, which is defined as:

$$De = \frac{1}{2}Re \sqrt{\frac{r}{r_{curvature}}} \quad (2.7.12)$$

where Re is the Reynolds number and $r_{curvature}$ the radius of the vessel curvature [2]. The Dean- and Reynolds numbers are important dimensionless quantities in fluid mechanics to predict turbulence and flow patterns inside fluid flows. The increase in fluid resistance due to vessel curvature is commonly preferred to that of smaller vessel radius. Modelling becomes successfully more complicated since vessel geometry also change during the heart cycle. This may be the vessel- and curvature radii, like in the aorta arch, as well as the cross-sectional area, as in bifurcations [2].

Compliance is mainly the result of vessel wall elasticity, having one active and one passive component. The passive elasticity derives from the vessel walls cell structure and elastin/collagen-ratio, while the active elasticity is associated with the smooth muscle cells within the vessel media [2]. As a unit, compliance is defined as the areal increase at a certain pressure change:

$$C = \frac{\Delta A}{\Delta P} \quad (2.7.13)$$

This relationship is, however, not completely linear. As described in section 2.4, vessel stiffness increases with higher pressure due to a progressively larger influence of the vessel walls collagen fibres [2].

The hemodynamic properties of blood also play a vital role in impedance modelling. Fluid resistance and inertia are, as described in equations (2.7.10) and (2.7.11), both proportional to the blood viscosity and density respectively. Blood is, however, not a true Newtonian fluid since its properties change with flow velocity. This is further complicated when considering very small vessels, such as the capillaries, where the diameter is equal to the size of the blood cells [2].

With the mechanical properties now defined and translated into the impedance model, the relationships of characteristic impedance and

PWV described in equations (2.7.7) and (2.7.9) may be rewritten as

$$Z_0 = \sqrt{\frac{L}{C}} = \sqrt{\frac{\rho\Delta P}{A\Delta A}} \quad (2.7.14)$$

$$c = \frac{1}{\sqrt{LC}} = \sqrt{\frac{A\Delta P}{\rho\Delta A}} \quad (2.7.15)$$

The expressions above are, apart from any reservations related to non-linearities, useful in the sense of showing how physical changes interact to affect the impedance pattern. It is also possible to transform the vascular system into an electrical model due to the close relationship in terminology between electrical- and vascular impedance, which has been done in models with varying complexity. The difficulty is as much of finding an appropriate model as to determine adequate model parameters since the system is, strictly speaking, non-linear [2].

2.7.3 Units of impedance modulus

The impedance modulus is, despite for longitudinal impedance, defined by equation (2.4.9) and is the quotient of the modulus of pressure (dyne/cm^2) and the modulus of flow (cm/s or cm^3/s). If expressed in cm/s or cm^3/s , the flow modulus is referred to as linear flow and volumic flow respectively. The impedance modulus may thus be expressed in $\text{dyne}\cdot\text{s}/\text{cm}^3$ or $\text{dyne}\cdot\text{s}/\text{cm}^5$ if linear- or volumic flow is used respectively [2].

Dyne is an old unit of force. It is defined as the force required for accelerating a 1 g mass at a rate of 1 cm/s^2 . It is a unit of the old centimetre-gram-second (CGS) system, a system preceding the modern SI-system [19]. By transferring the concept of dyne into the modern SI-

system, 1 *dyne* is equal to:

$$1 \text{ dyne} = 1 \text{ g} \cdot \text{cm}/\text{s}^2 = 10^{-5} \text{ kg} \cdot \text{m}/\text{s}^2 = 10^{-5} \text{ N} \quad (2.7.16)$$

To make the issue with units even more complicated, there is no standardized agreement or convention in literature on what expression that preferably should be used. In early theoretic treatment of arterial flow, in line with the coherence in electrical- and vascular systems, flow was considered as a velocity of flow (linear flow). This since the electrical analogy to flow, current, is treated as a velocity flow. In addition, impedance modulus in terms of linear flow (*dyne*·s/cm³) and units is analogous to both mechanical and acoustic impedance. The units are thus completely interchangeable after multiplication or division with the vessels cross-sectional area. However, more recent use of volumic flow has been done to express the impedance modulus (*dyne*·s/cm⁵). This is intuitive since the flow within the arterial system is considered in terms of a volumic flow [16].

2.7.4 Longitudinal impedance

Longitudinal impedance (Z_L) was the first vascular impedance to be defined in 1955, derived from equations describing motion in a thin-walled, liquid-filled tube. The concept of vascular impedance would later be broadened by successfully introducing the other terms of vascular impedance as well [16].

In contrast to the other forms, longitudinal impedance is the relationship between the pressure gradient ($P_1 - P_2$) and flow (Q). Longitudinal impedance is thus the opposition to flow along a segment of the artery, being only dependent on local properties of the vessel and the blood within it and not at all influenced by the vascular bed downstream. It has, among other things, been used to estimate the arterial pulsatile flow from the pulsatile pressure gradient recorded in

the artery. Longitudinal impedance is given in *impedance per unit length* l of the vessel by:

$$-\frac{\partial P}{\partial l} = \frac{P_1 - P_2}{l} = A^* e^{j\omega t} \quad (2.7.17)$$

where $A^* = M(\cos(\phi) - i \sin(\phi))$, M is the modulus of the complex conjugate A^* and ϕ its phase angle [16]. A graphical representation is given in **Figure 2.14** below.

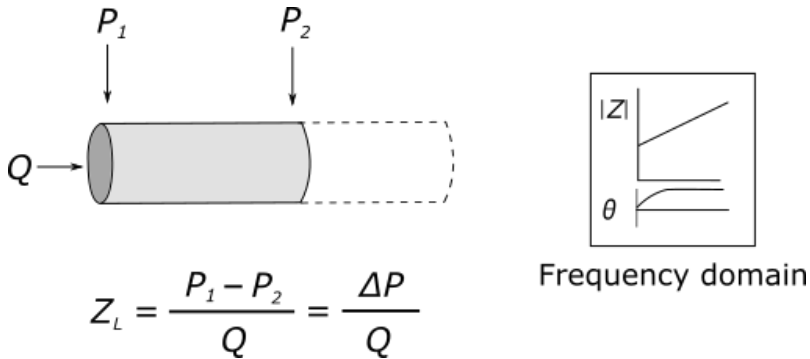


Figure 2.14: Diagrammatic- (left) and frequency domain (right) representations of longitudinal impedance. Inspiration from Nichols et al. [16].

Additionally, longitudinal impedance at zero frequency is equal to the longitudinal resistance, the relationship between mean pressure and flow along the length of the vessel [16].

The flow is expressed as:

$$Q = \frac{A^* \pi r^4 M'_{10}}{i \mu \alpha} e^{\varepsilon_{10}} e^{j\omega t} \quad (2.7.18)$$

where M'_{10} is the Bessel function modulus of the first kind and zero order, ε_{10} is the phase angle of the Bessel function and α the Womersley number [16]. The Womersley number is a dimensionless quantity in biofluid mechanics and biofluid dynamics, expressing the pulsatile flow frequency in relation to the fluids viscous effects as:

$$\alpha = r \sqrt{\frac{\omega\rho}{\mu}} \quad (2.7.19)$$

The longitudinal impedance may thus be expressed as:

$$Z_L = -\frac{\partial P}{\partial l} = \frac{A^* e^{j\omega t}}{Q} = \frac{i\mu\alpha^2 e^{-i\varepsilon_{10}}}{\pi r^4 M'_{10}} \quad (2.7.20)$$

which may be rewritten as:

$$Z_L = \frac{\mu\alpha^2}{\pi r^4 M'_{10}} \sin(\varepsilon_{10}) + \frac{i\mu\alpha^2}{\pi r^4 M'_{10}} \cos(\varepsilon_{10}) \quad (2.7.21)$$

From electrical engineering, the real- and imaginary parts of equation (2.7.21) corresponds to the resistive and reactive parts defined in (2.7.1). Thus:

$$R = \frac{\mu\alpha^2}{\pi r^4 M'_{10}} \sin(\varepsilon_{10}) \quad (2.7.22)$$

and

$$X = \frac{\mu\alpha^2}{\pi r^4 M'_{10}} \cos(\varepsilon_{10}) \quad (2.7.23)$$

From equation (2.7.19), equations (2.7.22) and (2.7.23) can be

rewritten as:

$$R = \frac{\omega\rho}{\pi r^2 M'_{10}} \sin(\varepsilon_{10}) \quad (2.7.24)$$

and

$$X = \frac{\omega\rho}{\pi r^2 M'_{10}} \cos(\varepsilon_{10}) \quad (2.7.25)$$

In this way, inductance may be expressed as:

$$L = \frac{\rho}{\pi r^2 M'_{10}} \cos(\varepsilon_{10}) \quad (2.7.26)$$

The inductance, *inertance per unit length of the vessel*, may be used to estimate the force per area associated with the acceleration of the fluid. This is done by multiplying the inductance with the flow velocity ($\frac{dQ}{dt}$).

2.7.5 Characteristic impedance

Vascular- and transmission line theory does, as described in section 2.7.1, show many resemblances. These resemblances are true to some extent but not, however, entirely. Transmission lines are, in theory, ideally treated as uniform and infinitely long. The transmission line does thus not experience any wave reflections from its other end or, at least, it is so long that wave reflections are very small in comparison with the forward propagating alternating current (AC) wave. Characteristic impedance is, in the sense of transmission lines, defined as the ratio between voltage and current of a single propagating wave along the line. The wave in question is traveling in one direction with

no wave reflections traveling in the other direction.

Characteristic impedance (Z_0) is thus, from its definition, the relationship between pulsatile pressure and pulsatile flow in the absence of wave reflections within the vascular system. This is, of course, not true for the vascular system. There is, in fact, no circumstance in life where pressure- and flow waves in arteries are unaltered by wave reflections. Instead, wave reflections are always present by-product from a series of contributors in the vascular system, but particularly due to the steep rise in vascular resistance in the

muscular arterioles. The vascular systems branching pattern and the varying properties of the vascular bed along its length is also contributors to the presence of wave reflections [16].

Despite the shortcomings regarding its definition, characteristic impedance has been frequently studied to characterize arteries and vessels. One explanation to this is the close correlation between characteristic impedance and PWV [16].

Characteristic impedance estimations have been considered in a variety of ways. A common way of estimating characteristic impedance has been to use the input impedance (to be described in section 2.7.6) modulus. This may be done either by averaging the impedance modulus over a frequency band where fluctuations due to wave reflections are present or by averaging the impedance modulus at high frequencies where any fluctuations from wave reflections have settled. The general idea is, in both cases, that any fluctuations above and below the characteristic impedance will cancel each other out. These approaches have, however, their practical shortcomings [16].

Another method to estimate characteristic impedance in the vascular system is to study the relationship between the initial upstroke of the pressure wave and the upstroke of the simultaneous flow wave. This

method assumes that any effects from wave reflections are either absent or minimal within approximately 40 ms of both waves. This method has proven fairly accurate when both local pressure- and flow waves are simultaneously measured at the same site [16].

Yet another method is to study the input impedance modulus when the vascular bed is maximally dilated, e.g. with medicinal injections, which reduces wave reflections to a minimum and, thus, approximates the characteristic impedance [16].

It is also possible to estimate characteristic impedance by separating the wave components of pulsatile pressure and pulsatile flow, permitting just the incident components to be related to each other [16, 20].

Like resistance and terminal impedance (to be described in section 2.7.7) is characteristic impedance commonly considered only in terms of modulus. This is because the phase being close to zero across the frequency range [16]. A graphical representation is given in **Figure 2.15** below.

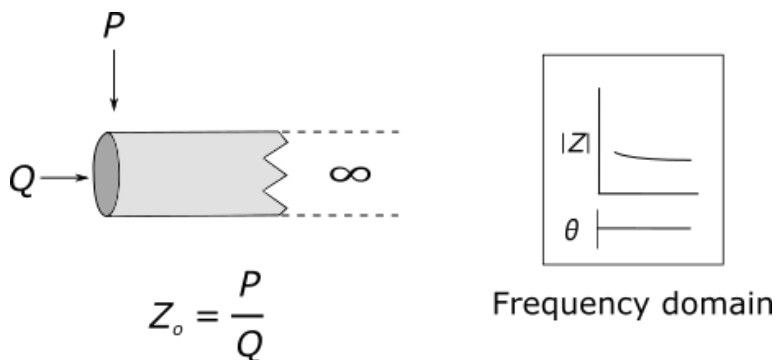


Figure 2.15: Diagrammatic- (left) and frequency domain (right) representations of characteristic impedance. Inspiration from Nichols et al. [16].

Input- and characteristic impedance are closely related, being continuations on the concept of longitudinal impedance. Just as the pressure gradient is related to absolute pressure, so is longitudinal impedance related to input impedance through complex wave velocity ($\frac{c}{i\omega}$). The simplest first case is to consider a system where wave reflections are absent (c). This gives the relationship between longitudinal- and characteristic impedance:

$$Z_0 = \frac{P}{Q} = \frac{P_1 - P_2}{Q} \frac{c}{i\omega} \quad (2.7.27)$$

or

$$Z_0 = Z_L \frac{c}{i\omega} \quad (2.7.28)$$

The relationship between characteristic impedance and arterial properties becomes clear by inserting equation (2.7.20) into equation (2.7.28), which gives:

$$Z_0 = \frac{c}{\omega} \frac{\mu \alpha^2 e^{-i\varepsilon_{10}}}{\pi r^4 M'_{10}} \quad (2.7.29)$$

or

$$Z_0 = \frac{c \rho e^{-i\varepsilon_{10}}}{\pi r^2 M'_{10}} \quad (2.7.30)$$

The expression of equation (2.7.30) may be rewritten one step further. Since arteries may be considered as longitudinally constrained tubes, c may be substituted for a relation that constrains the wave velocity c_0 by

$$c = \frac{c_0(M'_{10})^{1/2}}{(1 - \sigma^2)^{1/2}e^{-\varepsilon_{10}/2}} \quad (2.7.31)$$

where σ is Poisson's ratio. Equation (2.7.30) may thus be rewritten as:

$$Z_0 = \frac{c_0\rho e^{-i\varepsilon_{10}/2}}{\pi r^2(1 - \sigma^2)^{1/2}(M'_{10})^{1/2}} \quad (2.7.32)$$

From equation (2.7.32), it becomes clear that characteristic impedance varies directly with arterial elastic modulus and inversely with arterial

cross-sectional area. It is thus not strange that arteries with stiffer arterial walls and smaller vessel radii also exhibit higher characteristic impedance readings [16].

The theoretically predicted properties have been proven consistent through experimental testing, e.g. on femoral- and common carotid arteries of dogs. These determinations show a frequency dependent impedance modulus with no distinct fluctuations, combined with a phase being close to zero at all frequencies [16].

2.7.6 Input impedance

Whenever reflected waves are present in an impedance system, being either electrical or vascular, the situation becomes more complicated. This is due to the formation of nodes and antinodes between the signals within the system. The impedance at the origin of this system, which includes wave reflections, is referred to as input impedance (Z_i) [16].

In electrical- and transmission line theory, input impedance of an electrical network is the opposition to flow into a load bearing network

being external to a driving electrical source.

In vascular system theory, input impedance is the relationship between pulsatile pressure and pulsatile flow in a specific location of the arterial system. This measurement may thus be regarded as the input to all of the vascular bed beneath, not only dependent on the local arterial properties but also on properties of all vessels beneath until a point where the pulsations have attenuated, e.g. the arterial end of the capillaries. In this sense may input impedance from the ascending aorta be seen as the input impedance of the whole systemic arterial system. And in a similar manner may input impedance seen from the femoral artery express the input impedance of the femoral bed beyond [16]. A graphical representation is given in **Figure 2.16** below.

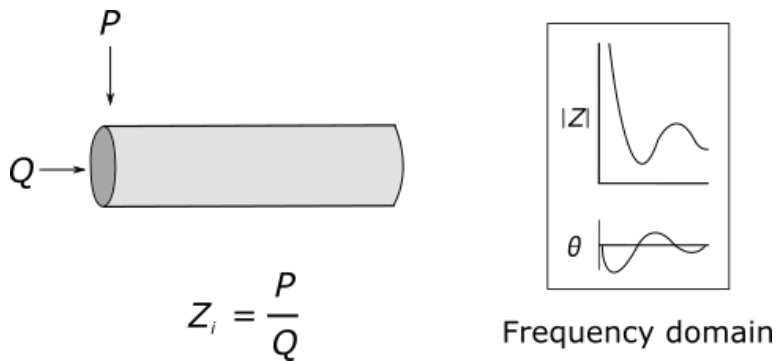


Figure 2.16: Diagrammatic- (left) and frequency domain (right) representations of input impedance. Inspiration from Nichols et al. [16].

Both longitudinal- and input impedance may be expressed in terms of modulus and phase. The longitudinal impedance modulus is, however, much smaller than that for input impedance. This is due to the longitudinal impedance being determined from the much smaller pressure gradient, over a limited length of the artery, instead of the

complete pressure wave as for the input impedance [16].

The input impedance modulus of any region in the arterial tree is the ratio of the pressure- and flow wave harmonics; whereas the input impedance phase is determined by the phase angle difference between the pressure- and flow waves [16].

The harmonic components of pressure and flow are given in complex notation by:

$$P = |P|e^{i(\omega t - \phi)} \quad (2.7.33)$$

and

$$Q = |Q|e^{i(\omega t - \beta)} \quad (2.7.34)$$

where ω is the angular velocity, ϕ the phase of pressure and β the phase of flow. The input impedance is thus, for a specific harmonic term, given by

$$Z_i = \frac{P}{Q} = \frac{|P|e^{i(\omega t - \phi)}}{|Q|e^{i(\omega t - \beta)}} = \frac{|P|e^{i(\beta - \phi)}}{|Q|} \quad (2.7.35)$$

which may be rewritten as:

$$Z_i = \frac{|P|}{|Q|} \cos(\beta - \phi) + i \frac{|P|}{|Q|} \sin(\beta - \phi) \quad (2.7.36)$$

From the real part of equation (2.7.36), the input impedance modulus is defined as:

$$|Z_i| = \frac{|P|}{|Q|} \quad (2.7.37)$$

and the input impedance phase as:

$$\theta = \beta - \phi \quad (2.7.38)$$

The input impedance has been of immense value in circulation- and arterial system studies. In relation to the other defined types of vascular impedance, even though they are important in their own ways, input impedance is deemed superior. Furthermore, where terms of “impedance” or “vascular impedance” are used without further definition, it is often taken to mean input impedance [16].

2.7.7 Terminal impedance

In transmission line theory, terminal impedance (Z_T) is referred to the impedance measured at the output terminals of a transmission line without any load and when no signals are transmitted through it [21].

In a similar manner for the vascular system, terminal impedance is defined as the opposition to flow at the termination of a vascular bed directly upstream from this termination, commonly represented by the high-resistive arterioles. In fact, resistance completely dominates reactance in the arterioles due to the minimal presence of blood inertia and vessel dispensability. Terminal impedance is thus considered in terms of modulus only [16]. A graphical representation is given in *Figure 2.17* below.

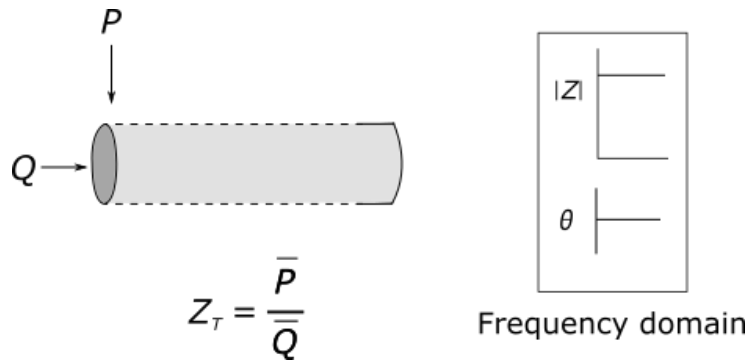


Figure 2.17: Diagrammatic- (left) and frequency domain (right) representations of terminal impedance. Inspiration from Nichols et al. [16].

It is the ratio between mean pressure and mean flow and is in many ways similar to peripheral resistance. It is, however, not strictly identical to peripheral resistance. Due to the finite drop in pressure along the arterial system and the finite pressure inside the capillaries, terminal impedance is somewhat smaller than peripheral resistance in amplitude. Peripheral resistance is calculated from the mean arteriovenous pressure difference, which is of considerable interest when venous pressure is high. This is normally occurring in the pulmonary system and during heart failure in the systemic circulation [16].

2.8 Diagnosis from vascular impedance patterns

As have been mentioned earlier, vascular impedance is mainly affected by three factors:

1. The geometry of the arterial tree.
2. The elastic properties of the arterial walls.
3. The density and viscosity of the blood.

From the appearance of the impedance pattern alone, it is not possible to separate the individual contributors. However, several cardiovascular pathological conditions may still be identified by the looks of the impedance pattern since it portrays itself in very characteristic ways. This interpretation is centred on four features listed below and visually illustrated in **Figure 2.18** below [2].

- a) The impedance level at zero frequency.
- b) The location of the first impedance minima.
- c) The average high frequency impedance level.
- d) The amount of oscillations at higher frequency.

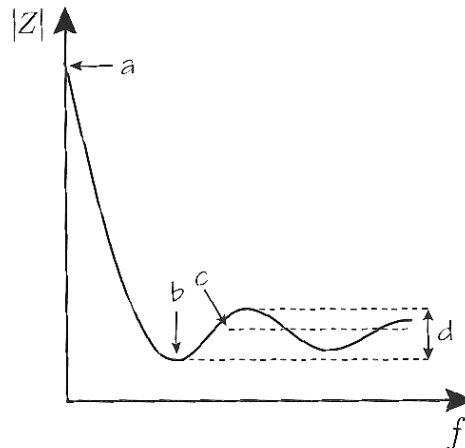


Figure 2.18: Interpretation of features in the input impedance pattern. Used with permission from Eriksson A. [2].

The impedance level at zero frequency, shown in *a*) above, is equal to the vessels peripheral resistance. The first impedance minimum, shown in *b*), is related to the closest major reflection site within the arterial system. The average high frequency impedance level, shown in *c*), may be used to estimate the characteristic impedance, which is based on the fact that reflected high frequency waves are heavily attenuated. And lastly, the high frequency oscillation level shown in *d*) indicate the

amount of arterial tree reflections. Regarding pathological condition identification, features of considerable interest are the location of the first impedance minima, $f_{Z_{min}}$, the average high frequency level and oscillatory content in the impedance modulus curve [2].

An illustration of the potential change in input impedance modulus with different physiological states is shown in **Figure 2.19**.

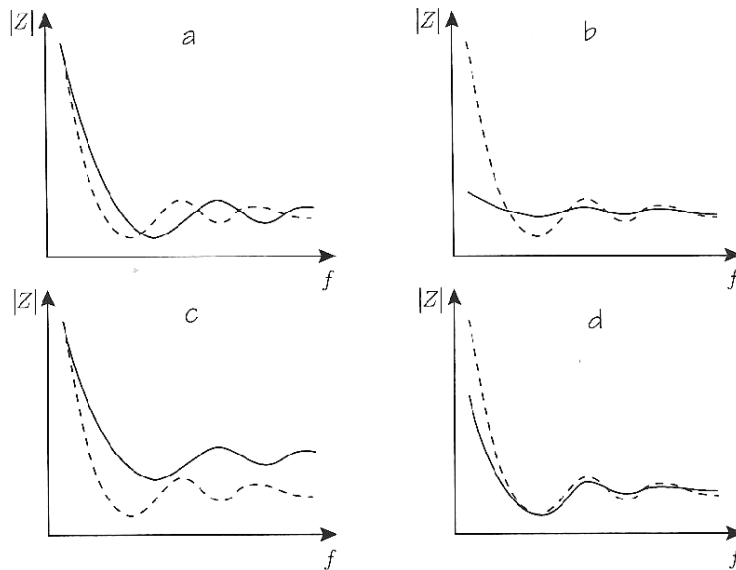


Figure 2.19: Typical impedance patterns of some physiological states. The dotted lines work as a normal reference. a) physical exercise b) Valsalva maneuver c) arteriosclerosis d) vasodilatation. Used with permission from Eriksson A. [2].

The heart rate is regulated in such a way that the location of the maximum energy in the frequency domain corresponds to the first impedance minimum. This is to minimize the left ventricular heart load. During exercise or stress, this impedance minimum is shifted to a higher frequency. Exercise increases both heart rate and aortic pressure, where the later causes cross-sectional area to increase and vessel

compliance to decrease. This in turn results in increased PWV according to equation (2.7.15). Because of the increased PWV within the vessel, the wave reflections start to return earlier; which corresponds to a higher $f_{z_{min}}$. In this way, low heart load is maintained despite the increased heart rate. By the same reasoning, followed by equation (2.7.14), does characteristic impedance not change considerably. And since the major reflection sites and the degree of reflections are the same as before, does the oscillatory behaviour remain almost unaffected [2].

The Valsalva maneuver is the praxis of attempted exhalation against closed airways. This is usually done by closing the mouth and pinching the nose shut while attempting exhalation as if inflating a balloon. This maneuver affects the circulatory system temporarily by increasing the intrathoracic pressure, which decreases the aortic cross-sectional area and the pressure across the vessel wall. By decreasing the pressure along the vessel wall increases the vessel compliance, which in return decreases PWV and $f_{z_{min}}$; whereas characteristic impedance remains the same. The result of this combination is an almost flat impedance spectrum, which indicates that wave reflections are significantly reduced [2].

Arteriosclerosis is the result of arterial wall thickening and stiffening. Similar to exercise does arteriosclerosis decrease vessel compliance, increase PWV and, consequently, increase $f_{z_{min}}$ in the impedance spectrum. But the cross-sectional vessel area does not increase in spite of the increased pressure and decreased vessel compliance. This indicates a different mechanism in play. In fact, as mentioned above, does arteriosclerosis change the very vessel wall structure; while wall stiffening due to increased pressure comes from the non-linear pressure-diameter relationship. Patients who suffer from arteriosclerosis also have a tendency to suffer from hypertension, which complicates the interpretation [2].

During vasodilatation are the smooth muscle cells within the media layer making the vessel wall to widen, which increases the arterial cross-sectional area. This decreases the low frequency components within the impedance spectrum. The oscillatory components also decrease due to a decrease in peripheral resistance. The opposite happens during vasoconstriction, where the smooth cells contract the vessel walls. This leads to higher low frequency impedance magnitudes and increasing wave reflections [2].

2.9 Input impedance as ventricular load and vascular power

When studying systemic and pulmonary circulations as a whole, input impedance of the ascending aorta and the main pulmonary artery is of considerable interest for understanding the systems interaction with the left and right ventricles respectively [16].

The ventricular ejection, i.e. the cardiac output, influence the amplitude and contour of the ascending aortic pressure- and flow waves as much as the properties of the systemic arterial system do. The ascending aortic impedance is furthermore regarded as the expression of the left ventricular hydraulic load. In a similar manner is the main pulmonary arterial impedance considered the work load of the right ventricle. By studying the vascular impedance in these arteries do not only give an understanding of their arterial properties; but also of the heart-vascular system interaction and their adaptation towards each other [16].

Ventricular afterload is a term used to describe the external vascular factors opposing ventricular systolic ejection. It is the resistance that the ventricles have to overcome to open. There is, however, no agreement on how to best characterize it. Some have suggested it to be the hydraulic input impedance presented to the ventricles, i.e.

ascending aortic input impedance to the left ventricle and main pulmonary arterial input impedance for the right ventricle. This suggestion has good argumentation behind it since input impedance and cardiac properties, which determine the pressure generated by ventricular ejection waves, are totally independent. There are, however, some difficulties connected to this concept and it has not gained popularity within the cardiac physiological- and cardiological societies [16].

Since impedance is comprised out of frequency dependent modulus- and phase spectra, there is no simple way of determining if it is increasing or decreasing by some intervention without quantifying the answer with specifications of the phase or frequency. The impedance modulus is furthermore given in units of pressure divided by flow (*dyne-s/cm⁵* or *dyne-s/cm³*), whereas afterload is given in units of force (*dyne*) or pressure (*dyne/cm²*). The concepts of arterial input impedance and ventricular afterload would thus be more useful if ventricular contraction also would be expressed in terms of its frequency content. The heart may be considered as a pressure- or flow generator connected in series with its source impedance being either the systemic- or pulmonary systems. This has been tested but, however, proved unhelpful through the considerable debates on whether the heart may be considered as a pressure- or flow source and to what degree the generator and source impedance are altered by myocardial contractual changes. The heart is, in contrast to the passive arterial system, an active pump whose properties change with time in systole and diastole.

This makes it impossible for the heart to be characterized in the frequency domain and further attempts have more or less been abandoned [16].

Ventricular afterload may thus be considered as an overly simplistic concept to be used on contracting ventricles. However, there is nothing denying that systemic- and pulmonary arterial input impedances

represent the hydraulic loads presented to left- and right ventricles respectively. Problems arise when trying to describe the ventricular functions in different situations. Apart from input impedance, some have used resistance whereas others have suggested characteristic impedance as the ventricular afterload; but they are nonetheless either adequate or completely appropriate to use since each is just another component of the input impedance. They also don't take into account for the fluctuations between peripheral resistance and characteristic impedance. Since wave reflections are of major significance to the values of modulus and phase, and indeed over the frequency range containing the ascending aortic flow waves major harmonic components; all three components – resistance, compliance and reflections – should be included when analysing the total ventricular external hydraulic load. All these components may be extracted from the input impedance spectrum [16].

Vascular power (W_v), also known in literature as external ventricular power, is the power generated by the ventricle that is lost as blood flows through the circulation [22]. The power consists of two components, one steady and one pulsatile component defined as:

$$W_v = W_s + W_p \quad (2.7.39)$$

The steady component (W_s) represents the power lost in steady flow through the peripheral resistance and the pulsatile component (W_p) to the arterial pulsations [23]. Furthermore, the pulsatile power is considered as wasted power whereas the steady power is useful power in driving the blood circulation within the arterial system. The steady

vascular power can be calculated through:

$$W_s = P_0 Q_0 \quad (2.7.40)$$

where P_0 and Q_0 are the mean arterial pressure and flow respectively; whereas the pulsatile vascular power is derived from:

$$W_p = \frac{1}{2} \sum_{n=1}^N Q_n^2 Z_{i_n} \cos \theta_n \quad (2.7.41)$$

where Q_n , Z_{i_n} and θ_n are the harmonic components of flow, input impedance modulus and input impedance phase respectively [16].

The external ventricular power is the hydraulic power imparted to the blood by the ventricle, but lost as the blood flows through the cardiovascular system. This power bears no constant relationship to the total ventricular power or to the myocardial oxygen need. These are largely determined by the pressure needed to be generated by the ventricles and thus by the developed- and sustained tension during systole of the ventricular muscle. In that sense, external ventricular power is more relevant to the cardiovascular systems than to the ventricles. The ratio between pulsatile- and total external ventricular power is thus a useful index of arterial (in)efficiency, but maybe not more than the difference in ascending aortic mean systolic- and mean diastolic pressure [16]. But by measuring the external ventricular power in two different locations in the cardiovascular system, the power lost in the regional vascular system may be estimated.

3. Method

3.1 Pre-existing *in vivo* recordings

Previous to the thesis project, a series of *in vivo* ultrafast plane wave ultrasound recordings of the right common carotid artery had been collected and stored in the department's digital database. They had been used beforehand by e.g. Albinsson *et al.* [24] to study longitudinal movement within the arterial wall. They consisted of 4 s long recordings sampled with a frame rate of 1.5 kHz, i.e. 6000 frames in total á recording. Each frame consisted of 64 scanlines, covering a 12.8 mm segment of the artery. It was originally meant for the radial motion tracking of this thesis project to be performed on these recordings as well.

However, a few months into the project, it became clear that the recordings were inadequate in quality for the purpose of this thesis project. Through thorough and careful evaluations, it was concluded that echo instability and the lacked of an incident pulse wave within the recordings were the main causes for the inadequacy. Brand new recordings had thus to be collected for the project to proceed.

3.2 New measurements and beamforming

For the new measurements, a next generation ultrasound machine (ULA-OP 256) was borrowed for 24 hours from the Department of Information Technology, University of Florence. ULA-OP stands for Ultrasound Advanced Open Platform and is an ultrasound machine specifically designed for research purposes. Its properties can be specifically tuned to fit its intended use through the open source

platform software it operates on. The system is illustrated in *Figure 3.1* below.



Figure 3.1: The ULA-OP 256 system [25].

The new measurements were performed on April 14:th 2018. Special personnel from SUS with extensive experience of performing ultrasound measurements were invited to assist during the measurements. For the measurements, two linear array probes were used: LA435 and LA533, Esaote, Genoa, Italy.

With the ULA-OP 256 system, a new set of *in vivo* ultrafast ultrasound recordings were taken of the right common carotid artery in eight healthy volunteers. Five men and three women of varied ages participated as volunteers. During the measurements, volunteers were lying down and resting. At the end of each volunteer session, blood

pressure measurements were collected together with data regarding the volunteers age and weight.

Both ultrafast plane wave- and compound imaging measurements were performed. In total, 57 ultrafast recordings were taken; 40 through plane wave imaging and 17 through compound imaging. Each frame consisted of 96 scanlines, covering a 19.2 mm segment of the artery. Frame rates of 5 and 7 kHz were used to guarantee capture of the incident pulse wave. Sadly, due to the sheer size of data, the recordings were limited to last only 1.7 or 2.4 s; corresponding to 1.5 or 2.5 cardiac cycles respectively.

The *in vivo* plane wave imaging recordings were beamformed over the coming month by using software from Alessandro Ramalli, PostDoc at the Catholic University of Leuven [26]. Only plane wave imaging recordings were used during this thesis project. After careful inspection and consideration, the best plane wave recording from each volunteer was chosen for a complete PWV- and vascular impedance analysis. An example of one such *in vivo* recording was previously illustrated in **Figure 2.4**.

The remaining parts of the thesis project consisted of programming in Matlab, MathWorks, Natick, MA, USA.

3.3 Motion tracking

Since PWV- and vascular impedance estimations are critically dependent on the performance of radial tracking of anterior- and posterior arterial wall movement, considerable time and effort was put into developing and evaluating the motion tracking results. Three motion tracking methods were utilized, one previously existing and two newly designed for this thesis project alone.

It was originally intended for a graphical user interface (GUI) to be designed along with the motion tracking methods. The program and its associated prototype GUI was provided by Cinthio M. at the start of the thesis project. After considerable modifications and development, the GUI was used during motion tracking and early vascular impedance estimations. However, due to several aspects, the design of the GUI was put on hold for the rest of the thesis project.

A brief description of the three utilized tracking methods: zero crossing-, phase shift- and iterative phase shift tracking, will now follow.

3.3.1 Zero crossing-tracking

The zero crossing (ZC) -tracking method is an ultrasound tracking method designed by Cinthio M. that was originally intended for this thesis project. It utilizes the zero crossings within RF-data for its motion tracking. The echoes within the RF-data will between successive frames, along with their zero crossings, move slightly depending on the recorded motion. Thus, by tracking the zero crossings of a strong echo, the motion of a physical structure may be tracked and estimated. The concept of ZC-tracking is illustrated in *Figure 3.2* below.

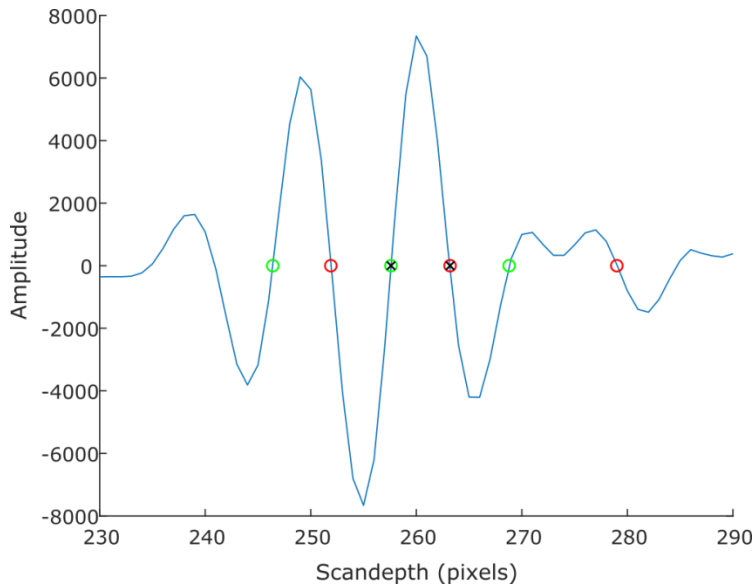


Figure 3.2: RF-signal with marked zero crossings. The echo being tracked is marked by X: s.

The ZC-tracking method is a principally simple and intuitive approach for motion tracking within ultrasound data. It is also a computationally fast tracking method, which was the first tracking method to be tested and evaluated. However, due to instability in the ultrasound echoes that gave raise to jumps in the final motion signals, it was not further evaluated.

3.3.2 Phase shift-tracking

Unlike ZC-tracking, phase shift (PS) -tracking utilizes phase shift between successive frames in IQ-data to track motion. An illustration of how a signal phase shift during motion is given in **Figure 3.3**.

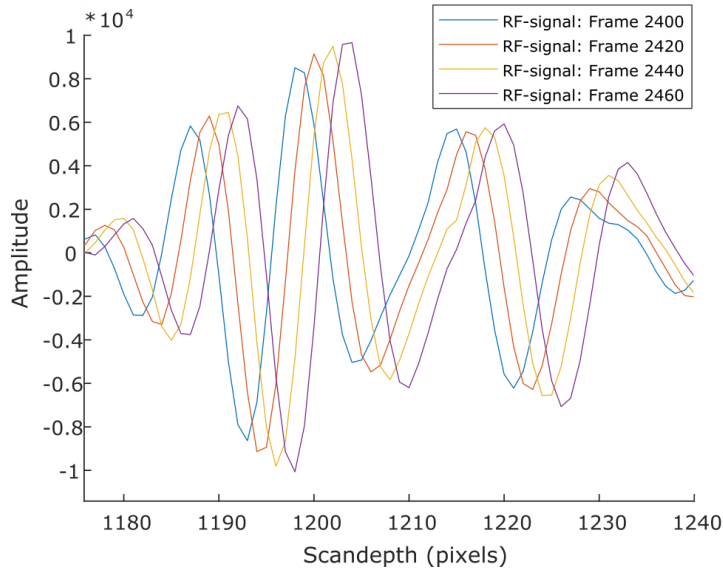


Figure 3.3: Part of RF-signal where its phase changes with movement in different frames.

The PS-tracking method was considerably more stable in regard to the echo stability than the ZC-tracking method, resulting in no potential jumps in the tracked arterial diameter movement signals. However, PS-tracking is considerably more demanding computationally than ZC-tracking. The tracked vessel movement also exhibits small amplitude ripple and a tendency of amplitude drift due to accumulated calculation errors in the phase estimations as the signal progresses with time.

3.3.3 Iterative phase shift-tracking

In an attempt to improve the performance of the PS-tracking method, two different means of motion tracking were combined, each used by their respective department employee. It is the hybrid combination between block matching used by Albinsson J. (Ph.D), and PS-tracking used by Erlöv T. (PostDoc). Hence, through this thesis project, the

iterative phase shift (IPS)-tracking method was born.

It uses the same type of phase-based motion estimation algorithm as the PS-tracking method mentioned above. But instead of utilizing phase shift between successive frames, it performs an iterative jumping action over a segment of frames of a predetermined size. An illustration of the iterative jumping process between frames can be seen in **Figure 3.4** below.

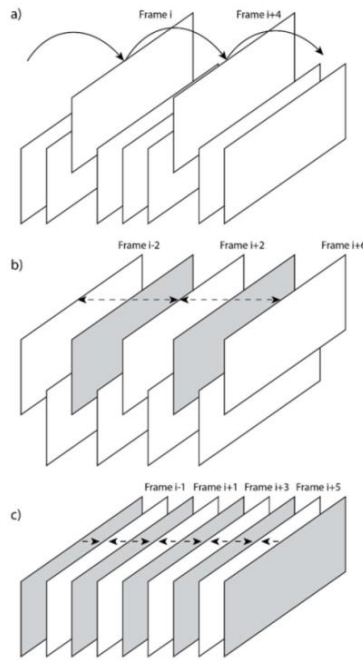


Figure 3.4: The iterative jumping process between distant frames of the IPS-tracking method. Used with permission from Albinsson J. [24].

The tracking process starts by calculating the phase difference between the first and last frames within the frame segment:

$$\Delta\phi_{1,N} = \phi_N - \phi_1 \quad (3.3.1)$$

where ϕ denotes the phase of the signal within a specific frame and N the predetermined frame segment size. Note that N is an uneven number related to the twofold relation:

$$N = 2^n + 1 \quad (3.3.2)$$

where n is the level above successive frames. The phase in frame N is then stored as equation (3.4.1):

$$\phi_N = \Delta\phi_{1,N} \quad (3.3.3)$$

For every successive decrease level of frame spacing, the differential phase shift between specifically distant frames within the frame segment is then calculated through:

$$\Delta\phi_{i-2^n,i} = \phi_{i-2^n} - \phi_i \quad (3.3.4)$$

and

$$\Delta\phi_{i+2^n,i} = \phi_{i+2^n} - \phi_i \quad (3.3.5)$$

where i denotes the frame being investigated. The final phase shift of frame i is then calculated through:

$$\phi_i = \Delta\phi_{i+2^n,i} - \Delta\phi_{i-2^n,i} \quad (3.3.6)$$

This process is repeated until the phase shift in every successive frame is calculated, which is later translated into motion displacement.

The IPS-tracking method has thus less accumulative calculation errors than the PS-tracking method and gives, theoretically, as a result, a better representation of the actual movement in the ultrasound

recordings. However, the execution time is longer than for PS-tracking. Also, unlike PS-tracking, IPS-tracking may potentially suffer from aliasing if the initial frame segment size N is set to high. If so, this number had to be decreased until no aliasing remained in the final arterial diameter traces from each scanline.

3.3.4 Performance evaluations

Method evaluations were performed on the newly designed PS- and IPS-tracking methods as a form of performance assessment. As a method evaluation, two parameters were investigated on the retrieved arterial diameter traces: ripple and trace variability.

Ripple is a small amplitude and high frequency oscillatory content, similar to noise, that was superimposed on the much larger arterial diameter traces. The amount of ripple was estimated in the arterial diameter trace for each scanline. The mean value and standard deviation (STD) of the ripple in each diameter trace were then calculated.

Trace variability refers to the tendency for a specific cardiac cycle location to vary, to some extent, in amplitude throughout the trace length. It may thus be regarded to as a measurement of the alignment between successive scanlines. Since the line density is five scanlines per millimetre, equalling a 0.2 *mm* distance between each scanline, the arterial diameter trace variability between successive scanlines should arguably be quite small; ideally being a smooth transition between scanlines. Depending on the arterial diameter trace appearance, systole or diastole amplitudes were compared. The trace variability was considered as follows:

- Amplitude in first occurring systole or diastole
- Amplitude in second occurring systole or diastole

- Differential amplitude between first and second occurring systole or diastole

The definitions stated above were extracted for each scanline. In the cases of first and second systole or diastole amplitudes, the derivative was also calculated. From the derivative of the first and second systole or diastole as well as the differential amplitude between first and second systole or diastole, the mean value and STD were calculated for each specific case.

3.4 Local pulse wave velocity estimations

Two methods were used to estimate the PWV in the ultrasound recordings: the pulse echo- and scatter plot techniques. Both techniques utilize the detection of vessel wall pulsations along a section of the artery. The general idea is to follow a specific location in the heart cycle in every scanline along the recorded section of the artery. It has become common practice to use end-diastole for PWV estimations since it marks the arrival of the forward propagating pulse wave. End-diastole is also referred to as “the foot” of the arterial diameter trace ($d_{L_1}(t)$, $d_{L_2}(t)$, $d_{L_3}(t)$, \dots , $d_{L_{N-1}}(t)$, $d_{L_N}(t)$) in each scanline. Examples of these arterial diameter traces are shown in *Figure 3.5* below.

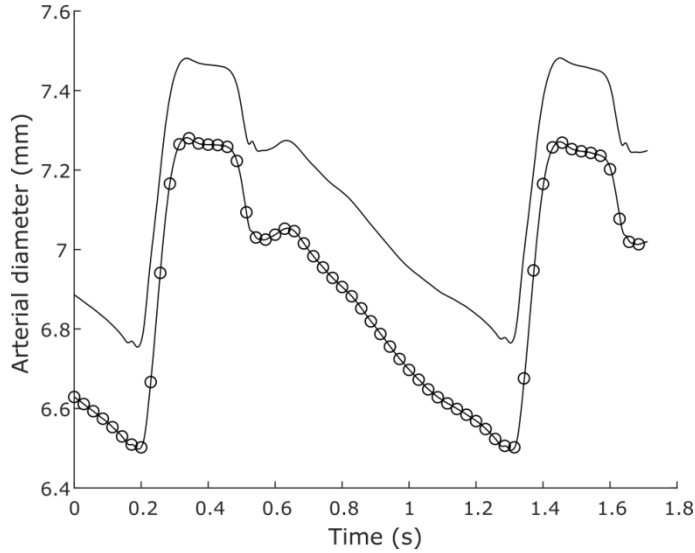


Figure 3.5: Example of arterial diameter change over time. The traces originate from the first (—) and last (\ominus) scanlines reached by the pulse wave.

In this thesis project, PWV estimations were performed on both the velocity- ($v_{L_1}(t)$, $v_{L_2}(t)$, $v_{L_3}(t)$, ..., $v_{L_{N-1}}(t)$, $v_{L_N}(t)$) and acceleration traces ($a_{L_1}(t)$, $a_{L_2}(t)$, $a_{L_3}(t)$, ..., $a_{L_{N-1}}(t)$, $a_{L_N}(t)$) of the tracked arterial diameter movement from each scanline. Examples of these differential wall velocity- and acceleration traces are shown in **Figure 3.6** and **Figure 3.7** below respectively.

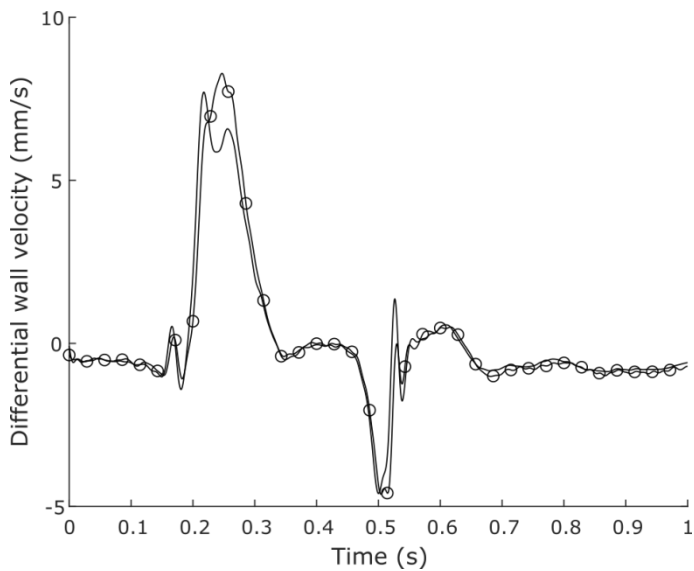


Figure 3.6: Partial differential wall velocity over time. The traces originate from the first (—) and last (⊖) scanlines reached by the pulse wave.

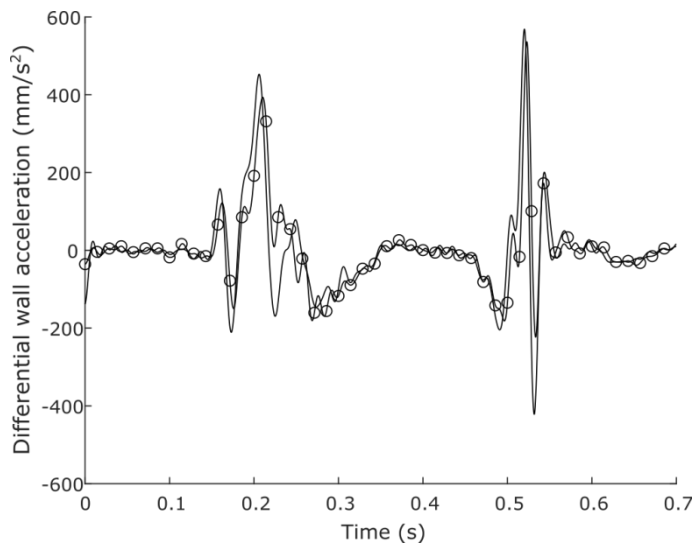


Figure 3.7: Partial differential wall acceleration over time. The traces originate from the first (—) and last (⊖) scanlines reached by the pulse wave.

For velocity traces, zero crossing positions corresponding to end-diastole in the diameter traces were used to estimate PWV. And in a similar manner, for the acceleration traces, peak acceleration positions were used since they correspond to the actual arrival of the incident pulse wave.

The pulse-echo technique is a commonly used method to estimate regional PWV in arteries from ultrasound recordings using ultrafast imaging technology. The PWV is thus obtained from the pulsation delay along the artery due to the finite wave pulsation. By fitting a linear curve of this location in every scanline, and based on the time-shift (Δt) and travel distance (Δx), local PWV is estimated. **Figure 3.8** illustrates the concept in a simple two scanline scenario.

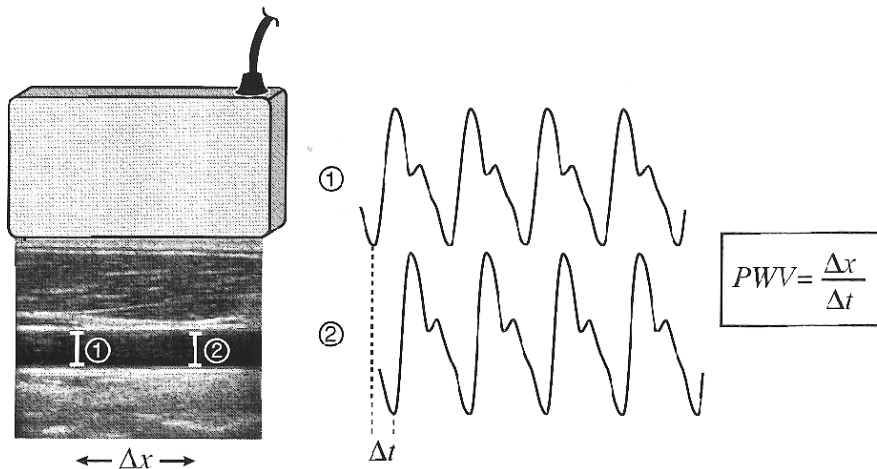


Figure 3.8: The pulse echo technique detecting vessel diameter pulsations in two scanlines along the artery. Used with permission from Eriksson A. [2].

The scatter plot technique was the method used by Eriksson *et al.* [2] to estimate local PWV from Tissue Doppler Imaging (TDI) recordings of the common carotid artery. It is, to some extent, similar to the pulse-echo PWV estimation technique, since it also utilizes a specific

location in the heart cycle for its PWV estimation. But instead of a straight forward linear estimation from the detected positions of the predetermined heart cycle location in every scanline, each heart cycle location in every scanline is compared to the same corresponding location in the successive scanline ($v_{L_1}(t)$ vs. $v_{L_2}(t)$, $v_{L_2}(t)$ vs. $v_{L_3}(t)$, \dots , $v_{L_{N-1}}(t)$ vs. $v_{L_N}(t)$) and ($a_{L_1}(t)$ vs. $a_{L_2}(t)$, $a_{L_2}(t)$ vs. $a_{L_3}(t)$, \dots , $a_{L_{N-1}}(t)$ vs. $a_{L_N}(t)$). This process is later repeated with progressively increasing line distance $l = 2, 3, \dots, N - 1$. In other words, ($v_{L_1}(t)$ vs. $v_{L_3}(t)$, $v_{L_2}(t)$ vs. $v_{L_4}(t)$, \dots , $v_{L_{N-2}}(t)$ vs. $v_{L_N}(t)$) as well as ($a_{L_1}(t)$ vs. $a_{L_3}(t)$, $a_{L_2}(t)$ vs. $a_{L_4}(t)$, \dots , $a_{L_{N-2}}(t)$ vs. $a_{L_N}(t)$) and so on. By successfully increasing the line distance, less possible scanline combinations are included. It is from these scanline combinations that a linear curve may be fitted to estimate the PWV. In this way, all possible trace combinations between scanlines are exploited which theoretically may improve the PWV estimation. The concept is illustrated in **Figure 3.9** below.

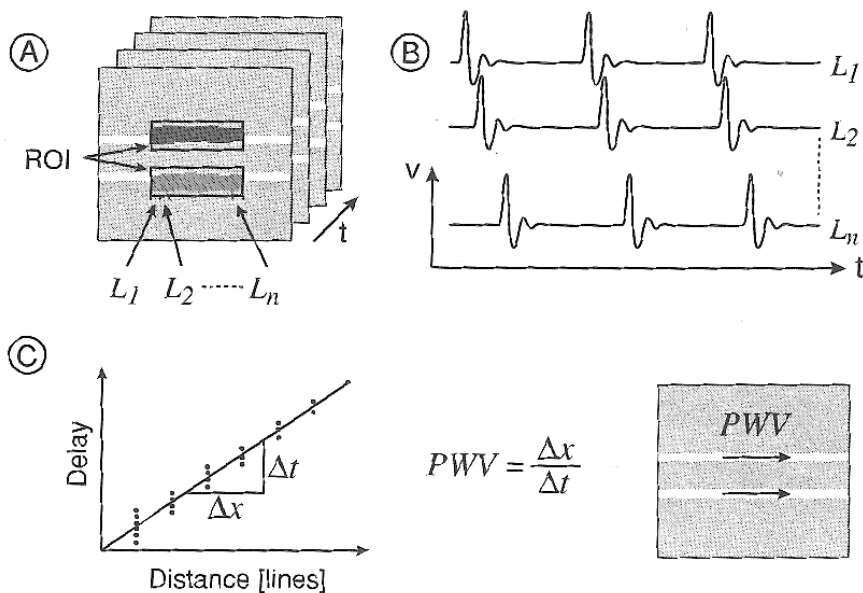


Figure 3.9: The scatter plot technique, in this case utilizing vessel wall velocities (B), for the PWV estimation. The vessel wall velocities are extracted from recorded tissue motion (A), from which the delays between velocity traces (C) are used to estimate the PWV. Used with permission from Eriksson A. [2].

For this thesis project, a modification of the Eriksson *et al.* scatter plot estimation was used. In this, velocity- and acceleration traces are analysed in a similar manner as before. The specific heart cycle location in every scanline was compared to the same corresponding location in the successive scanline ($v_{L_1}(t)$ vs. $v_{L_2}(t)$, $v_{L_2}(t)$ vs. $v_{L_3}(t)$, \dots , $v_{L_{N-1}}(t)$ vs. $v_{L_N}(t)$) and ($a_{L_1}(t)$ vs. $a_{L_2}(t)$, $a_{L_2}(t)$ vs. $a_{L_3}(t)$, \dots , $a_{L_{N-1}}(t)$ vs. $a_{L_N}(t)$). This process was repeated with progressively increasing line distance $l = 2, 3, \dots, N - 1$. In other words, ($v_{L_1}(t)$ vs. $v_{L_3}(t)$, $v_{L_3}(t)$ vs. $v_{L_5}(t)$, \dots , $v_{L_{N-2}}(t)$ vs. $v_{L_N}(t)$) as well as ($a_{L_1}(t)$ vs. $a_{L_3}(t)$, $a_{L_3}(t)$ vs. $a_{L_5}(t)$, \dots , $a_{L_{N-2}}(t)$ vs. $a_{L_N}(t)$) and so on.

The local PWV is often portrayed as a colour mapped image of adjacent velocity- or acceleration traces known as Pulse Wave Imaging (PWI). In this, the PWV is displayed as a gradual linear motion; representing the pulse waves arrival in different parts of the artery.

The tracking results were found not only to include an overall forward propagating pulse wave. Upon closer inspection, a backward propagating motion in both velocity- and acceleration traces were found. Caused by wave reflections, arriving approximately 50 ms after the forward propagating pulse wave, this motion was later identified, mathematically, to be the bifurcation reflected pulse wave. Hence, PWV estimations of both the incident- and reflected pulse waves were performed. For the bifurcation reflected pulse wave, both peaks were investigated for the velocity traces whereas both zero crossings and peaks were investigated for the acceleration traces.

3.5 Vascular impedance estimations

Similar to the work performed by Eriksson *et al.* [2], vascular impedance was estimated from the definition of characteristic impedance. Because of the influence of wave reflections in the arterial system, as illustrated in *Figure 1.4*, an estimate of the input impedance is accessible.

The wave velocity, as a function of frequency, may be estimated from utilizing the phase in each successive scanlines arterial diameter trace. Since the velocity is related to the phase, it is referred to as phase velocity (φ). The phase velocity is defined as:

$$\varphi(f) = \frac{\Delta x 2\pi f}{\Delta \theta(f)} \quad (3.5.1)$$

where Δx is the length of the arterial section covered by the scanlines, $\Delta \theta$ the difference in phase between all scanlines and f the frequency;

either the fundamental frequency, i.e. the heart rate, or one of its harmonics [2]. By plotting the phase in each scanlines arterial diameter trace, a linear increase (or decrease) in phase emerges. It is thus, from equation (3.6.1), the slope of this trend that determines the phase velocity in each frequency component.

Due to the limited amount of heart cycles contained in the *in vivo* recordings, the scanlines had to be combined to increase the energy content sent into the FFT. By combining the arterial diameter traces of even- and odd numbered scanlines respectively, i.e. $(d_{L_1}(t), d_{L_3}(t), d_{L_5}(t), \dots, d_{L_{N-3}}(t), d_{L_{N-1}}(t))$ and $(d_{L_2}(t), d_{L_4}(t), d_{L_6}(t), \dots, d_{L_{N-2}}(t), d_{L_N}(t))$, a decent estimation of the phase velocity was performed. The vascular impedance modulus was then estimated from:

$$|Z(f)| = \frac{\rho\varphi(f)}{\pi r^2 M'_{10}(\alpha)} \quad (3.5.2)$$

Viscosity μ and fluid density ρ were considered constant and chosen to those for blood (i.e. $\mu = 4.0 \text{ cP}$ and $\rho = 1050 \text{ kg/m}^3$) [2].

The phase velocity- and vascular impedance estimations were found sensitive and heavily dependent on the initial tracking points positioned in the arterial wall. In an effort to combat this, nine initial tracking positions along both the anterior- and posterior walls were simultaneously tracked. An illustration of this is given in **Figure 3.10** below.

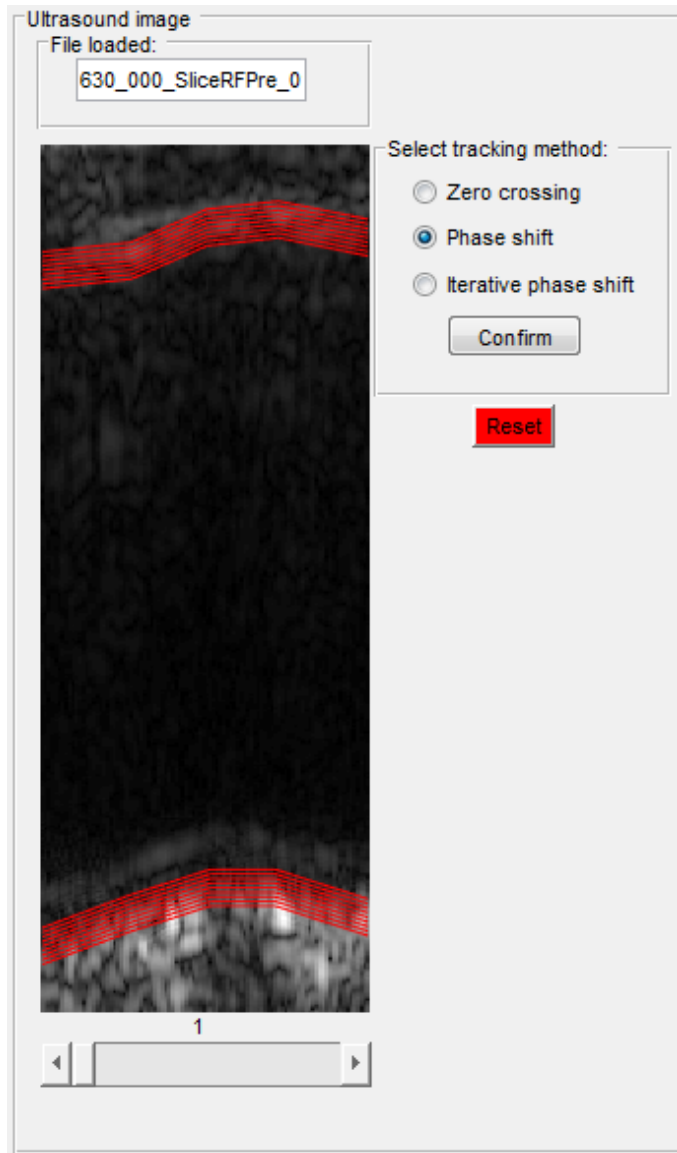
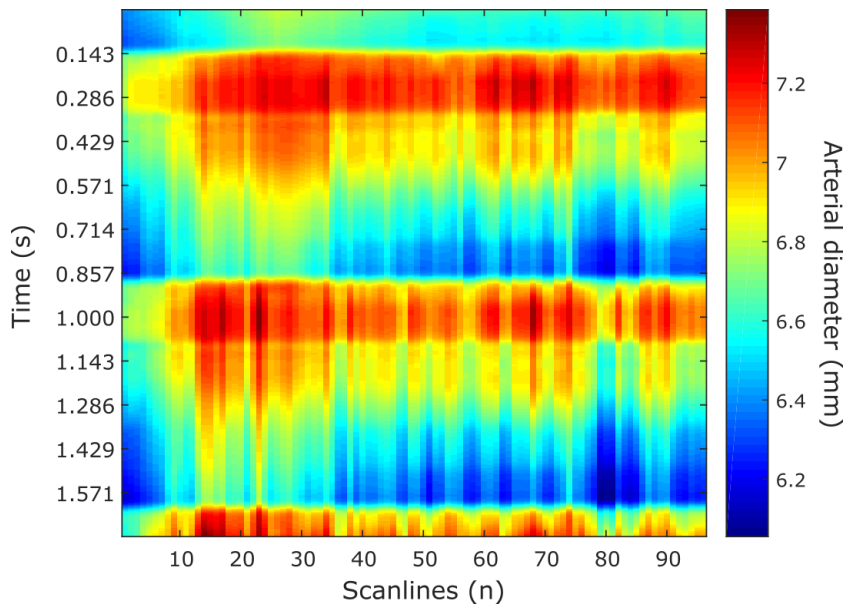


Figure 3.10: Part of the GUI used when initiating motion tracking by setting initial tracking positions and choosing what tracking method to be performed.

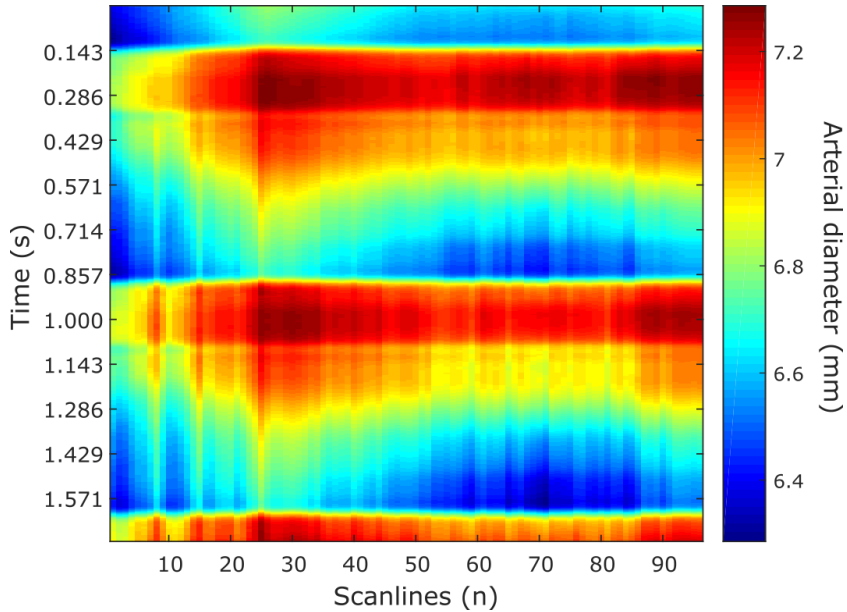
4. Results

4.1 Motion data

An example of the potential results from PS- and IPS-tracking is presented in *Figure 4.1* below. The pattern is consistent in every *in vivo* recording; where IPS-tracking produces smoother and more coherent transitions between arterial diameter traces in successive scanlines.



(a) PS-tracking results.



(b) IPS-tracking results.

Figure 4.1: Example of potential difference between PS- (a) and IPS- extracted arterial diameter traces (b).

4.2 Performance evaluations

Results of the ripple mean value- and STD-estimations in the tracked arterial diameter change traces are presented in **Table 4.1**. An illustration of the estimated ripple level in each scanline within an *in vivo* recording, from which the mean values and STD:s are estimated, is seen in **Figure 4.2**.

Table 4.1: Ripple estimate in the arterial diameter traces. Units are per cent of the arterial diameter displacement.

Test subject	PS-tracking		IPS- tracking	
	Mean value (%)	Standard deviation (%)	Mean value (%)	Standard deviation (%)
630	0.020	0.0035	0.024	0.0050
631	0.017	0.0032	0.018	0.0032
632	0.019	0.0040	0.022	0.0061
633	0.021	0.0015	0.022	0.0016
634	0.024	0.0047	0.027	0.0061
635	0.032	0.010	0.032	0.0088
636	0.047	0.0081	0.052	0.0090
637	0.012	0.0017	0.014	0.0035

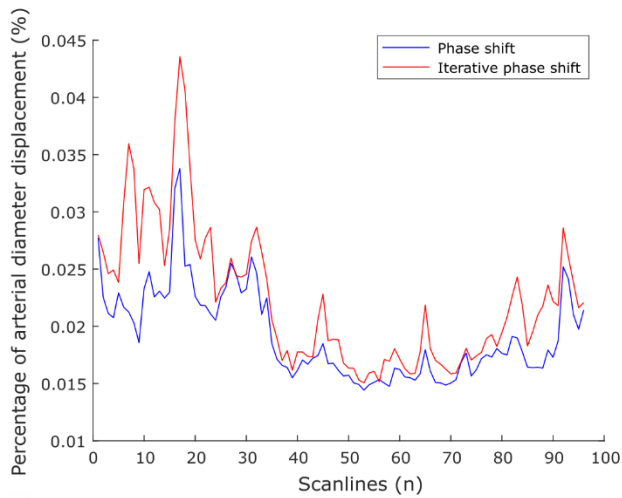


Figure 4.2: Example of ripple present within each scanline in PS- and IPS-tracking results.

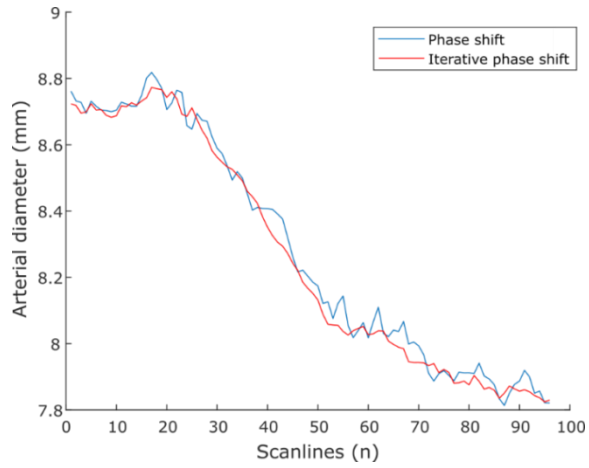
Results of the arterial diameter amplitude variability mean value- and STD-estimations are presented in **Table 4.2**, **Table 4.3** and **Table 4.4**. With each table, an illustrative example is displayed of the arterial diameter in first diastole in **Figure 4.3**, second diastole in **Figure 4.4** and their differential amplitude in **Figure 4.5**.

Table 4.2: Arterial diameter amplitude variability in first peak systole or end diastole. Units are millimetres per scanline.

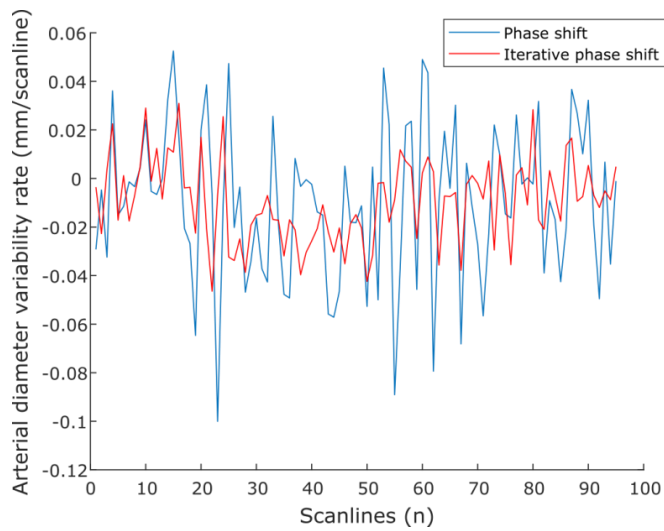
Test subjects	PS-tracking		IPS- tracking	
	Mean value (mm/scanline)	Standard deviation (mm/scanline)	Mean value (mm/scanline)	Standard deviation (mm/scanline)
630*	0.00028	0.018	-0.00021	0.012
631**	-0.0037	0.018	-0.0039	0.017
632*	-0.0068	0.014	-0.0071	0.0089
633*	0.0024	0.014	0.0021	0.012
634**	-0.0099	0.032	-0.0094	0.017
635*	-0.0033	0.044	-0.0039	0.021
636*	0.0054	0.086	0.0072	0.033
637**	-0.0022	0.015	-0.0024	0.014

*: Peak systole

** : End diastole



(a) Arterial diameter in first end diastole.



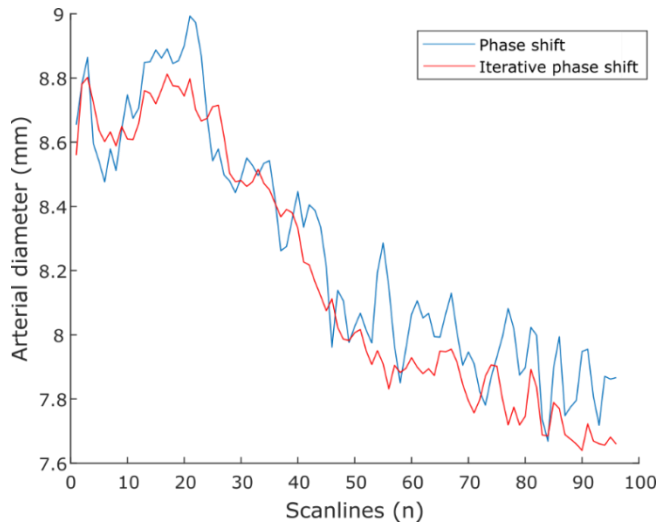
(b) Arterial diameter variability rate in first end diastole.

Figure 4.3: Example of arterial diameter and variability rate in first end diastole.

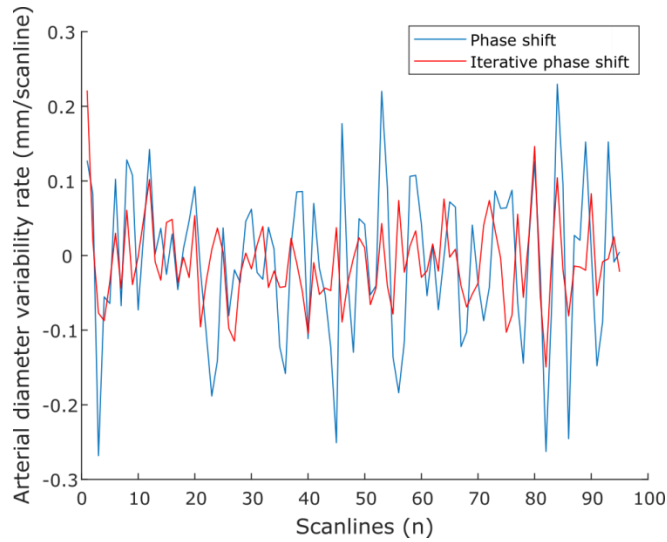
Table 4.3: Arterial diameter amplitude variability in second peak systole or end diastole. Units are millimetres per scanline.

Test subject	PS-tracking		IPS- tracking	
	Mean value (mm/scanline)	Standard deviation (mm/scanline)	Mean value (mm/scanline)	Standard deviation (mm/scanline)
630*	0.00069	0.035	-0.00040	0.019
631**	-0.0032	0.029	-0.0039	0.027
632*	-0.0066	0.024	-0.0072	0.014
633*	0.0025	0.021	0.0022	0.014
634**	-0.0083	0.10	-0.0092	0.058
635*	-0.0025	0.074	-0.0034	0.041
636*	0.0052	0.10	0.0064	0.043
637**	-0.0015	0.027	-0.0021	0.018

*: Peak systole
 **: End diastole



(a) Arterial diameter in second end diastole.



(b) Arterial diameter variability rate in second end diastole.

Figure 4.4: Example of arterial diameter and variability rate in second end diastole.

Table 4.4: Arterial diameter amplitude variability of differential amplitude between first and second peak systole or end diastole. Units are millimetres per scanline.

Test subject	PS-tracking		IPS- tracking	
	Mean value (mm/scanline)	Standard deviation (mm/scanline)	Mean value (mm/scanline)	Standard deviation (mm/scanline)
630*	0.02	0.028	0.027	0.017
631**	-0.0043	0.025	0.00047	0.018
632*	-0.036	0.023	-0.037	0.012
633*	-0.00044	0.019	-0.0076	0.011
634**	-0.021	0.11	-0.082	0.070
635*	0.017	0.054	0.030	0.027
636*	-0.038	0.062	-0.050	0.052
637**	0.0089	0.033	0.020	0.014

*: Peak systole

** : End diastole

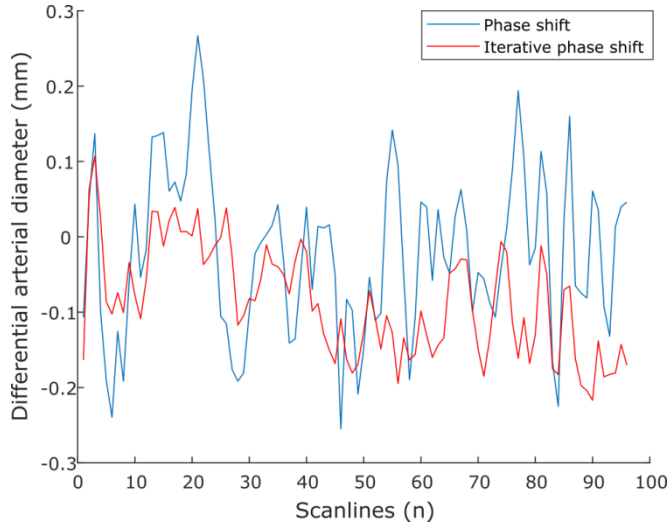


Figure 4.5: Example of differential arterial diameter between first and second end diastole.

Table 4.5: Factoral STD improvement ($= \frac{STD_{ps}}{STD_{ips}}$) in IPS-tracking results compared to PS-tracking results specified in Table 4.2 – 4.4.

Test subject	First peak systole or end diastole	Second peak systole or end diastole	Differential arterial amplitude
630*	1.5	1.8	1.7
631**	1.1	1.1	1.4
632*	1.6	1.7	1.9
633*	1.2	1.5	1.8
634**	1.9	1.8	1.5
635*	2.1	1.8	2.0
636*	2.6	2.4	1.2
637**	1.1	1.5	2.4

*: Peak systole

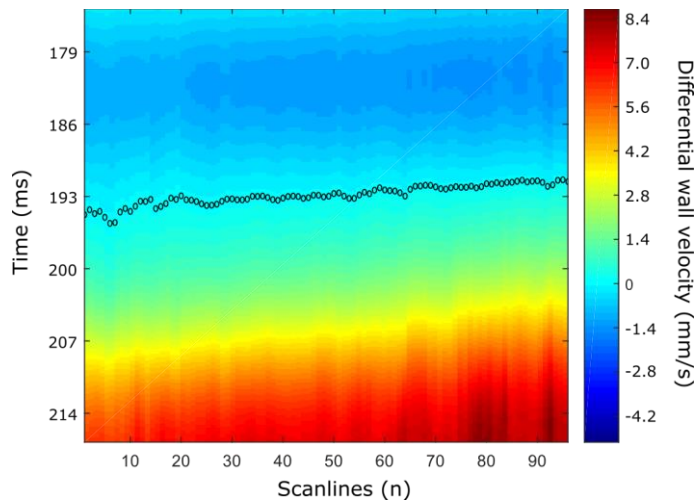
** : End diastole

From **Table 4.5**, IPS-tracking reduced STD in mean by a factor of 1.6, 1.7 and 1.7 in the first-, second- and differential amplitude between first- and second peak systole or end diastole respectively.

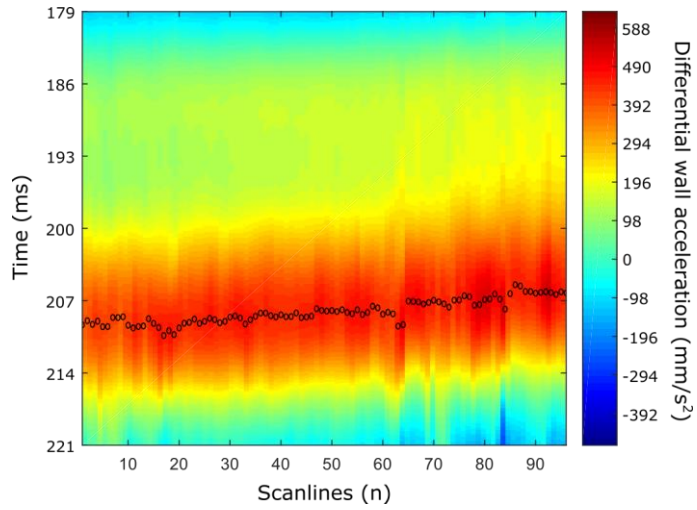
4.3 Local pulse wave velocity

4.3.1 Forward propagating pulse wave

For illustrative purposes, examples of PWV estimations in velocity- and acceleration traces through PWI with pulse-echo- and scatter plot techniques are shown in **Figure 4.6** and **Figure 4.7** respectively for the incident pulse wave. A summation of the PWV estimation results by using the pulse-echo technique is shown in **Table 4.6**, and the scatter plot technique in **Table 4.7**. The results in **Table 4.6** and **Table 4.7** are then visualized in separate plots based on use of tracking method, PWV estimation method, gender and tracing in **Figure 4.8**.

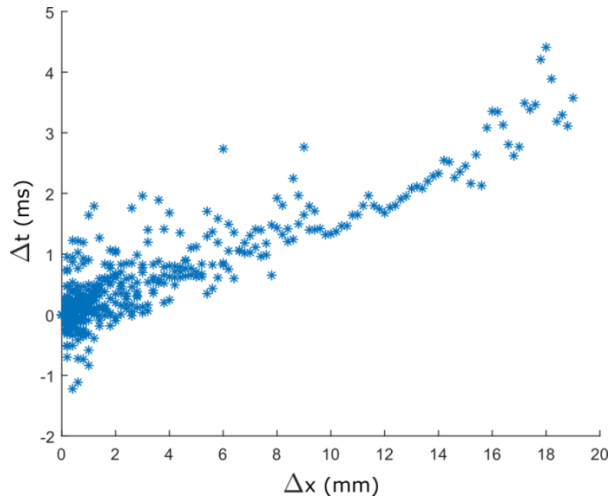


(a) Pulse-echo PWV estimation on zero crossings of IPS-extracted velocity traces.

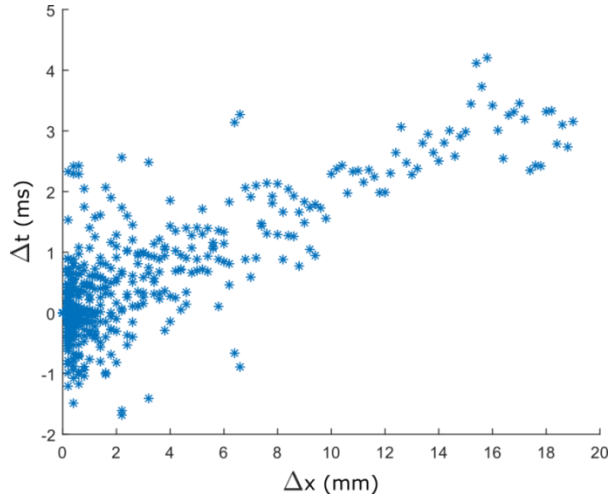


(b) Pulse-echo PWV estimation on peaks of PS-extracted acceleration traces.

Figure 4.6: PWI examples of pulse-echo PWV estimations of the incident pulse wave on velocity- (a) and acceleration traces (b). The PWV was estimated to 4.01 m/s and 5.69 m/s respectively in this case.



(a) Scatter plot PWV estimation on zero crossings in IPS-extracted velocity traces.



(b) Scatter plot PWV estimation on peaks of PS-extracted acceleration traces.

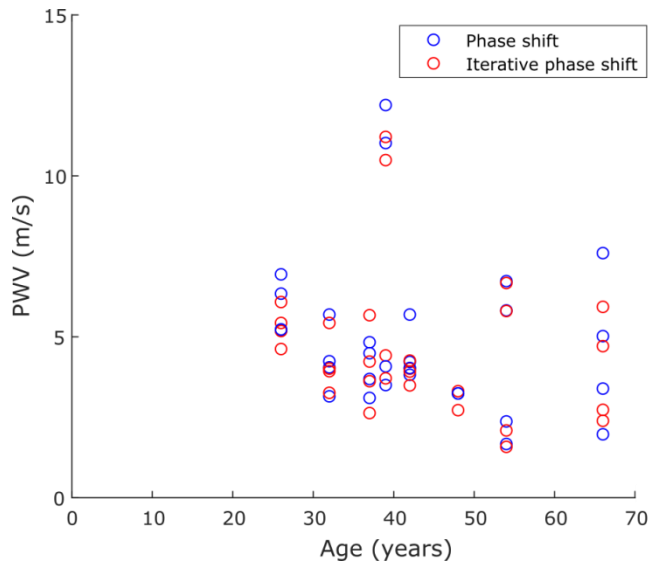
Figure 4.7: Examples of scatter plot PWV estimations of the incident pulse wave on velocity- (a) and acceleration traces (b). The PWV was estimated to 3.26 m/s and 4.24 m/s respectively in this case.

Table 4.6: Pulse-echo PWV estimations of the incident pulse wave. Units are metres per second.

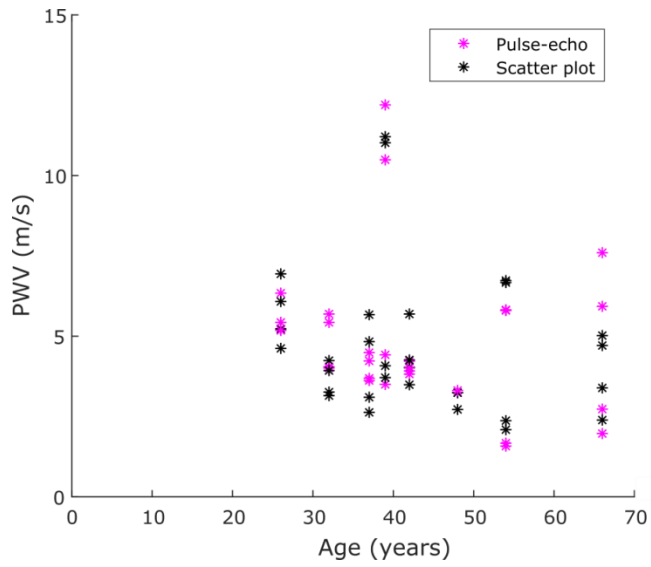
Test subject	PS-tracking		IPS-tracking	
	Velocity traces (m/s)	Acceleration traces (m/s)	Velocity traces (m/s)	Acceleration traces (m/s)
630	4.05	5.69	4.01	5.43
631	12.20	3.50	10.49	4.42
632	7.60	1.97	5.93	2.73
633	6.34	5.20	5.43	5.18
634	79.19	3.24	31.32	3.31
635	4.49	3.69	4.23	3.62
636	1.67	5.82	1.58	5.80
637	4.22	3.82	4.01	3.92

Table 4.7: Scatter plot PWV estimations of the forward propagating pulse wave. Units are metres per second.

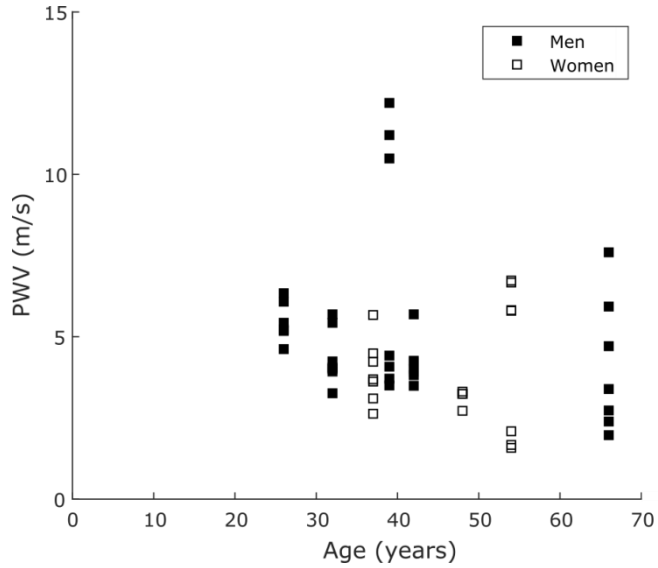
Test subject	PS-tracking		IPS-tracking	
	Velocity traces (m/s)	Acceleration traces (m/s)	Velocity traces (m/s)	Acceleration traces (m/s)
630	3.15	4.24	3.26	3.93
631	11.02	4.08	11.21	3.71
632	5.02	3.39	4.71	2.39
633	6.94	5.23	6.08	4.62
634	-14.13	3.24	-25.43	2.72
635	4.83	3.10	5.67	2.63
636	2.37	6.73	2.09	6.67
637	4.03	5.69	4.26	3.49



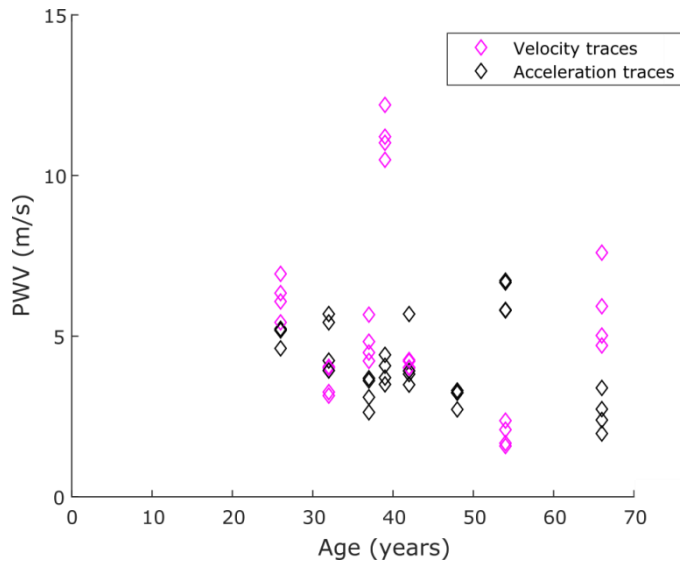
(a) PWV estimations based on PS- and IPS-tracking data.



(b) PWV estimations based on pulse-echo- and scatter plot estimations.



(c) PWV estimations based on gender.

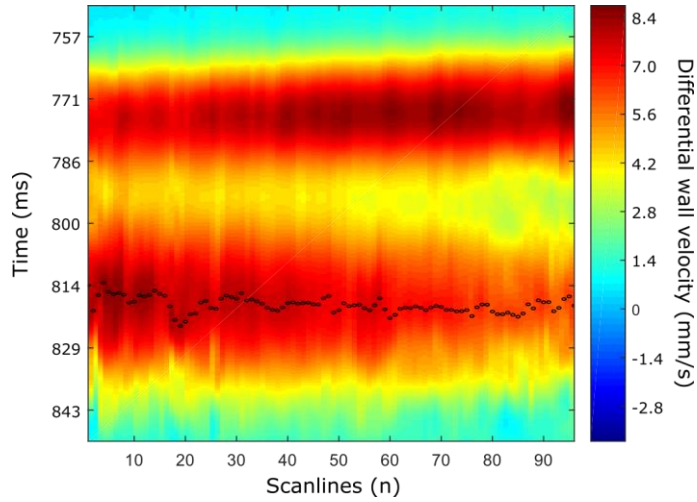


(d) PWV estimations based on velocity- and acceleration traces.

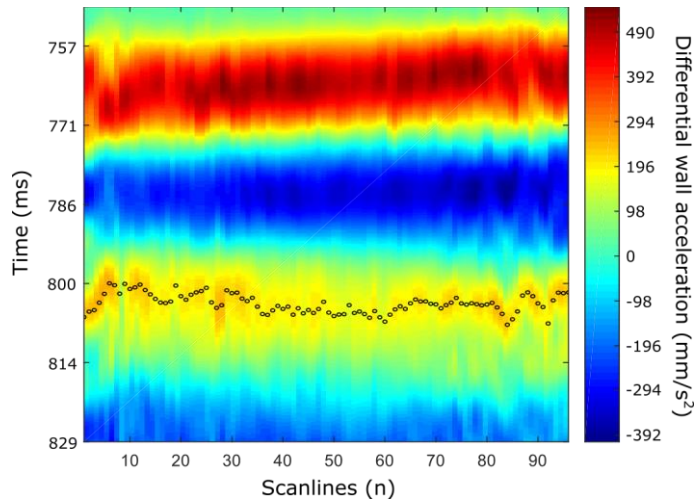
Figure 4.8: Visual representation of data in **Table 4.5** and **Table 4.6**, showing the most reasonable PWV estimations of the incident pulse wave.

4.3.2 Bifurcation wave reflection

As for the case of the incident pulse wave; illustrative examples of PWV estimations in velocity- and acceleration traces through PWI are given with pulse-echo- and scatter plot techniques in **Figure 4.9** and **Figure 4.10** respectively for the bifurcation wave reflection. A summation of the PWV estimations from the pulse-echo technique is shown in **Table 4.8** and **Table 4.10**; whereas the scatter plot technique results are given in **Table 4.9** and **Table 4.11**. The results in **Table 4.8** and **Table 4.9** are then visualized in separate plots based on use of tracking method, PWV estimation method, gender and tracing in **Figure 4.11**.

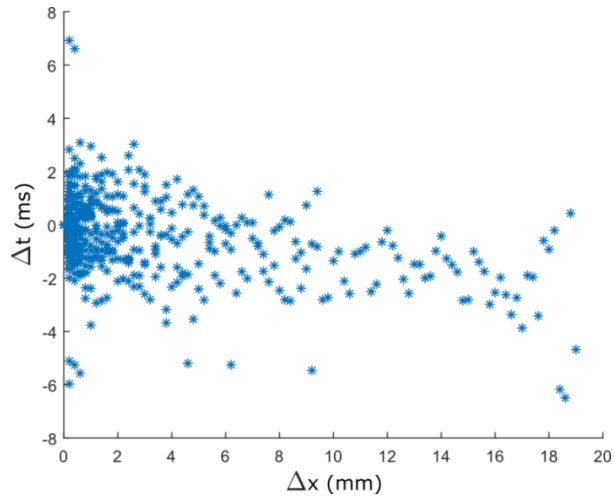


(a) Pulse-echo PWV estimation on peaks of IPS-extracted velocity traces.

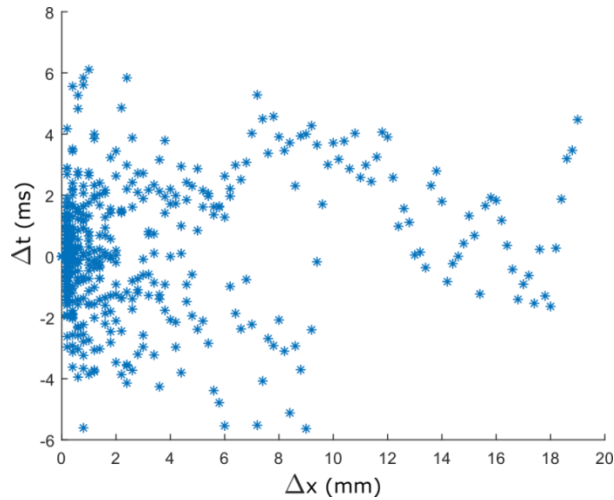


(b) Pulse-echo PWV estimation on peaks of PS-extracted acceleration traces.

Figure 4.9: PWI examples of pulse-echo PWV estimations of the bifurcation wave reflection in velocity- (a) and acceleration traces (b). The PWV was estimated to -4.44 m/s and -13.06 m/s respectively in this case.



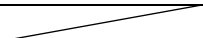
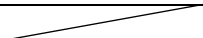
(a) Scatter plot PWV estimation on peaks of IPS-extracted velocity traces.



(b) Scatter plot PWV estimation on peaks of PS-extracted acceleration traces.

Figure 4.10: Examples of scatter plot PWV estimations of the bifurcation reflected pulse wave on velocity- (a) and acceleration traces (b). The PWV was estimated to -7.96 m/s and 44.91 m/s respectively in this case.

Table 4.8: Pulse-echo PWV estimations of the bifurcation wave reflection by using peaks in velocity- and acceleration traces. Units are metres per second.

Test subject	PS-tracking		IPS-tracking	
	Velocity traces (m/s)	Acceleration traces (m/s)	Velocity traces (m/s)	Acceleration traces (m/s)
630	-6.90	13.17	-8.63	5.41
633	-4.18	-4.44*	-5.27	-2.57*
634	-4.30	3.45*	-4.42	3.92*
635	-1.69		-1.74	
637	-4.44	-2.31	-5.44	-13.06

*: Estimated from half of the peak positions due to diffuse appearance in signals.

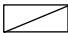
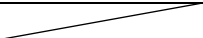
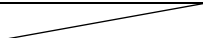
: Estimation incomplete due to internal trace instability.

Table 4.9: Scatter plot PWV estimations of the bifurcation wave reflection by using peaks in velocity- and acceleration traces. Units are metres per second.

Test subject	PS-tracking		IPS-tracking	
	Velocity traces (m/s)	Acceleration traces (m/s)	Velocity traces (m/s)	Acceleration traces (m/s)
630	-6.50	14.17	-13.30	5.84
633	- 2.05	-7.24*	10.10	-2.01*
634	-3.61	-1.06*	3.66	-1.10*
635	-2.25		-3.01	
637	-7.96	11.01	-10.75	44.91

*: Estimated from half of the peak positions due to diffuse appearance in signals

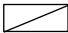
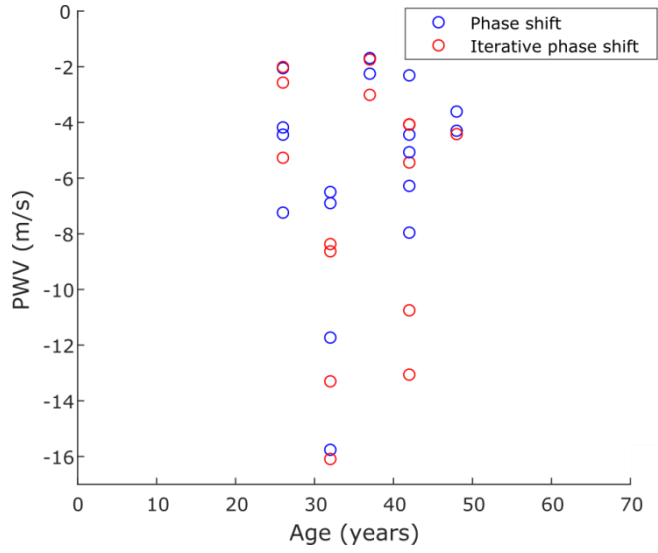
: Estimation incomplete due to internal trace instability.

Table 4.10: Pulse-echo PWV estimations of the bifurcation wave reflection by using zero crossings in acceleration traces. Units are metres per second.

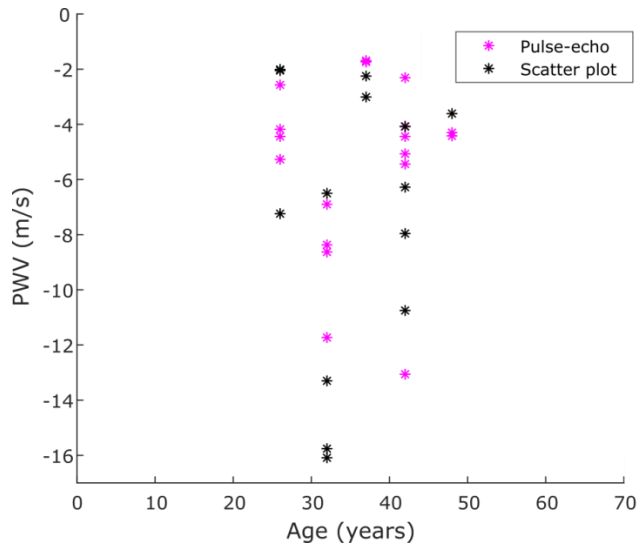
Test subject	PS-tracking	IPS-tracking
	<i>Acceleration traces (m/s)</i>	<i>Acceleration traces (m/s)</i>
630	-11.73	-8.37
637	-5.07	-4.07

Table 4.11: Scatter plot PWV estimations of the bifurcation wave reflection by using zero crossings in acceleration traces. Units are metres per second.

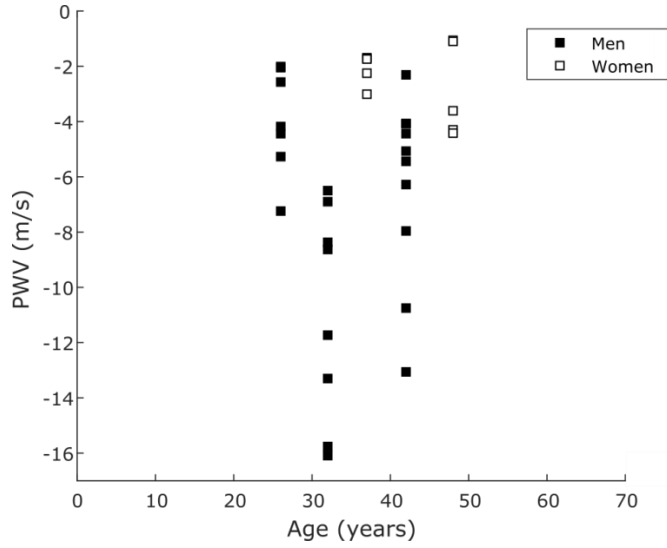
Test subject	PS-tracking	IPS-tracking
	<i>Acceleration traces (m/s)</i>	<i>Acceleration traces (m/s)</i>
630	-15.76	-16.09
637	-6.28	-4.01



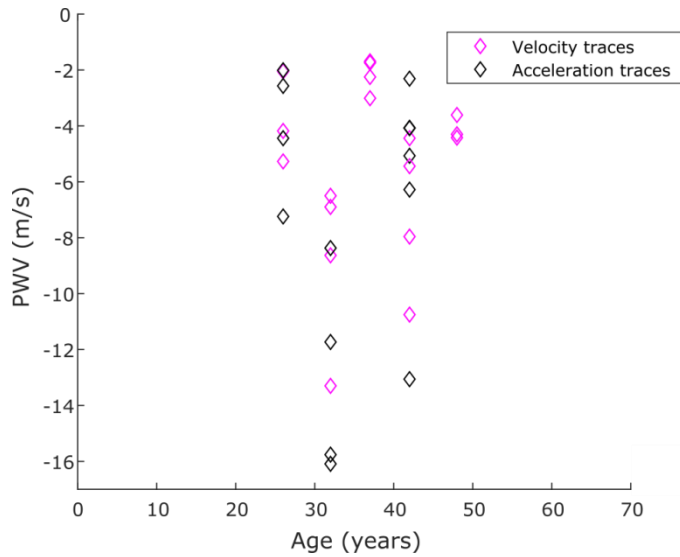
(a) PWV estimations based on PS- and IPS-tracking data.



(b) PWV estimations based on pulse-echo- and scatter plot estimations.



(c) PWV estimations based on gender.

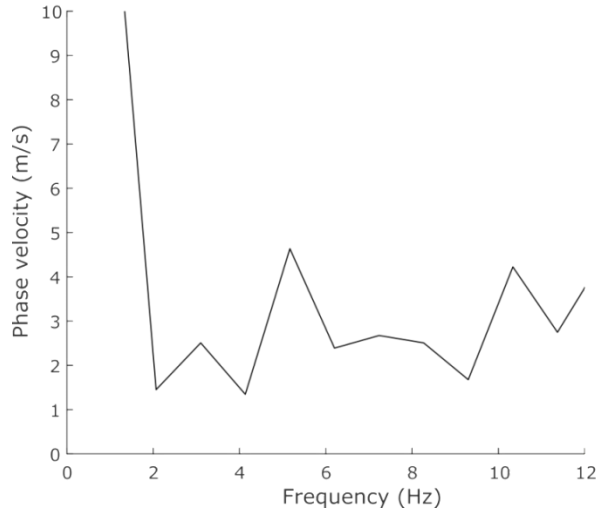


(d) PWV estimations based on velocity- and acceleration traces.

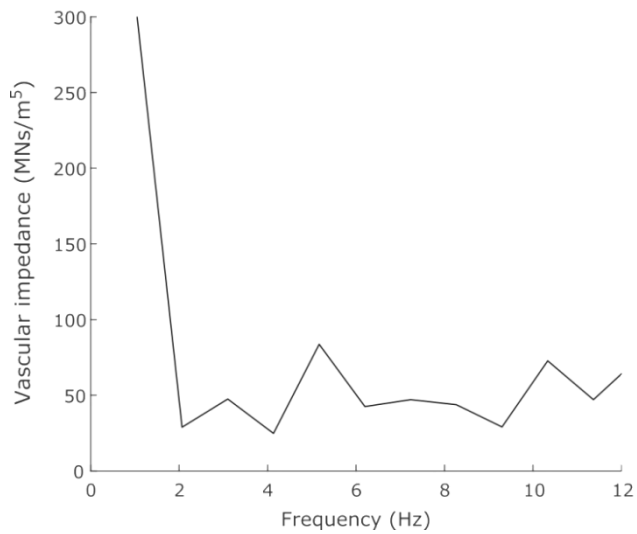
Figure 4.11: Visual representation of data in **Table 4.7** and **Table 4.8**, showing the most reasonable PWV estimations of the bifurcation wave reflection.

4.4 Vascular impedance

Out of the total number of recordings analysed, only two gave reasonable results in terms of phase velocity and vascular impedance component values. These are shown in *Figure 4.13* and *Figure 4.14* below.

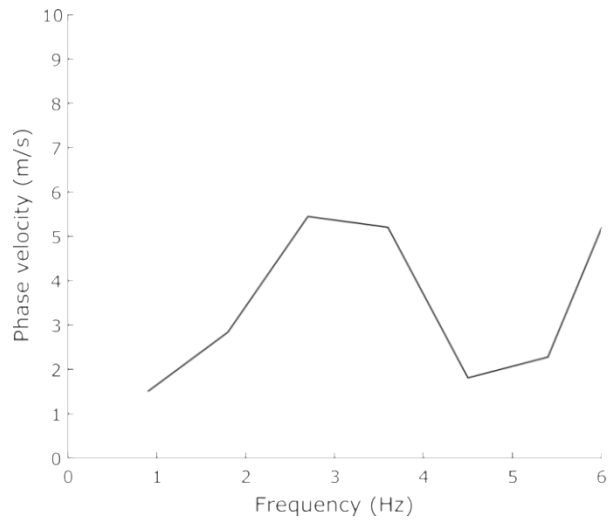


(a) Phase velocity profile from IPS-tracking data.

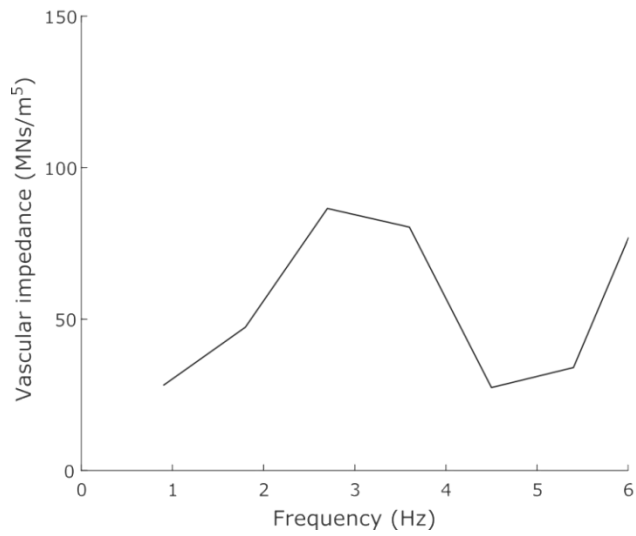


(b) Vascular impedance modulus from IPS-tracking data.

Figure 4.13: Phase velocity profile and vascular impedance modulus in volunteer 630.



(a) Phase velocity profile from PS-tracking data.



(b) Vascular impedance modulus from PS-tracking data.

Figure 4.14: Phase velocity profile and vascular impedance modulus in volunteer 633.

5. Discussion

Since the final PWV- and vascular impedance estimations were to be highly dependent on the quality of previously performed steps, a lot of time was invested in getting the groundwork, i.e. beamforming and motion tracking, to perform as good as possible. The process has, however, been toilsome.

5.1 Measurements and in vivo recordings

As mentioned in section 3.3, the recordings were limited to span just 1.7 or 2.4 s due to the maximized data storage capabilities of the ULA-OP 256 system. As a consequence, the amount of complete cardiac cycles within each recording was very limited, ranging from 1.5 to 2.5 depending on the frame rate. In spite of their limited time span, after being beamformed and compressed, one recording took 27 GB of storage space. To handle and process each recording during motion tracking to a reasonable extent, each recording was split into 20 sub files á 1.4 GB. Motion tracking was then performed on each sub file, continuously uploading them onto the computers Random Access Memory (RAM) and combining the tracking results from each sub file to create the total, coherent, motion signal. Due to the sheer size of each recording, PS- and IPS-motion tracking took a lot of time to perform. Also, due to the nature of ultrafast imaging recordings, any occasional troubleshooting was challenging. For further work in this field, a recommendation is to implement parallel programming by also utilizing the computers Graphical Processing Unit (GPU). The execution time for PS- and IPS-tracking would thus be reduced drastically.

The process was further hampered since the recording equipment, i.e. the ULA-OP 256 system, was lent from the Department of Information Technology, University of Florence, and only available for 24 hours. Thus, the chance of redoing any new ultrafast imaging recordings was not possible. Furthermore, it was a challenge to get recordings with good focus on both anterior- and posterior arterial walls simultaneously. From the limitations defined by the ultrasound recordings, every measure was taken to extract as much valuable information within the recordings as possible.

5.2 Motion tracking and performance evaluations

As mentioned in section 3.4.1, the ZC-motion tracking method was abandoned at an early stage due to its inbuilt sensitivity to echo instability within RF-data. Whenever echoes emerge or disappear within the proximity to the zero crossings being tracked, this may potentially cause abrupt changes in the zero crossings positions and is seen as “jumps” in the final extracted motion data. Since frequency analysis is a central component to both PWV- and vascular impedance estimations, such jumps are not desirable. This tracking method, however, should not be discarded in the future without further considerations. A potential solution exists by applying ZC-tracking on the compound imaging recordings which were also performed during the thesis project. These recordings combine frames taken with plane wave ultrasound beams from five different angles of incidence instead of one ultrasound beam as in plane wave imaging. After beamforming, compound imaging recordings contain less speckle, echo instability and other impurities; potentially to such an extent that ZC-tracking will perform desirably. But still, ZC-tracking remains a less robust tracking method than PS- and IPS-tracking.

At an early categorization stage, all ultrafast plane wave recordings were tracked with PS-tracking. Of those giving the smoothest motion traces, IPS-tracking was also applied. The final product would become the diameter traces from which both local PWV- and vascular impedance estimations would be based on. From the appearance of the diameter traces shown in section 4.1, those extracted with PS-tracking show less coherence between diameter traces than those extracted with IPS-tracking. Thus, based on the appearance of **Figure 4.1**, IPS-tracking gives better estimations of the arterial wall positions. However, given by the mean values of both ripple and trace variability in **Table 4.1 – 4.4**, IPS-tracking shows a higher amplitude differencing within its diameter traces than PS-tracking. Simultaneously, it shows more coherence along its successive scanlines. It is unclear why IPS-tracking displays higher level of ripple and trace variability in mean than PS-tracking. When replaying the tracking procedure of both methods, it is clear that IPS-tracking better follows the arterial to a smoother extent than PS-tracking. This is also supported by the STD estimations in **Table 4.1 – 4.4**. The question is, however, how accurate the assumption of a stable arterial diameter change with time really is. The body may very well be non-zeroed at all times, allowing the arterial diameter pattern level to alter slightly between cardiac cycles. But it is still fully reasonable to expect adjacent parts of the artery to be similar in amplitude, giving a smooth transition along the length of the artery. Thus, the performance evaluations performed on the PS- and IPS-tracking methods, shown in section 4.2, suggests better performance of IPS-tracking throughout. On the ultrasound recordings chosen for full analysis during this thesis project, STD was reduced by a factor of 1.6, 1.7 and 1.7 in the first-, second- and differential amplitude between first- and second peak systole or end diastole scenarios when using IPS-tracking. However, these numbers are based on the best recordings for each volunteer; supposedly making the performance evaluation more of a worst-case scenario rather than best-case scenario for IPS-tracking. IPS-tracking has more to gain when used on less stable ultrasound recordings, but is also more computationally demanding than PS-tracking. However, other

performance evaluation measures, e.g. of image smoothness, may be relevant to explore in the future.

5.3 Local pulse wave velocity estimations

For the incident pulse wave; local PWV estimations yielded reasonable and plausible results when compared with previous work published in the field [27, 28]. Regarding the most reasonable estimations in this thesis project, pulse-echo PWV estimations varied between 1.58 – 7.60 m/s in velocity traces and 1.97 – 5.82 m/s in acceleration traces; whereas scatter plot estimations yielded values varying between 2.09 – 6.94 m/s in velocity traces and 2.39 – 6.73 m/s in acceleration curves. It is known that PWV may vary greatly between individuals, increases naturally with age but earlier in men than in women. From **Table 4.6** and **Table 4.7**, as well as their visual representations in **Figure 4.8**, it is clear that PWV may vary greatly depending to the methodology applied to estimate it. The PWV estimations are clearly sensitive to the line fitting of the attained sample points, where even small variations in slope gives a high variance in PWV estimations. This is true for both the pulse-echo- and scatter plot techniques. However, the acceleration traces tend to give slightly less varying estimations than the velocity traces as shown in **Figure 4.8**. The quality of the ultrasound recordings and the motion tracking results are thus of high relevance to the outcome of and variability in PWV estimations. It is also possible for the PWV to vary within very small arterial sections, e.g. in the presence of plaque, stenosis or abdominal aortic aneurysm (AAA Sac). This has been proven through piecewise Pulse Wave Imaging (pPWI), where parts of the ordinary PWI-plot are separated based on changes in the otherwise homogenously pulse wave progression along the artery [29].

For the bifurcation wave reflection, PWV estimations yielded even more varying results. The presence of a wave reflection coming from

the right common carotid arterial bifurcation point has been known to exist for some time [27, 30]. Yet, it has not seemingly been estimated to any large degree in terms of its PWV. Since estimations of this wave reflections PWV is less known, more or less all negative values have been considered plausible (except for some extreme values). Through pulse-echo estimations, PWV values ranged between $-1.69 - 8.63$ *m/s* in velocity traces and $-2.31 - 13.06$ *m/s* in acceleration traces; whereas scatter plot estimations yielded values between $-2.05 - 13.30$ *m/s* in velocity traces and $-1.06 - 16.09$ *m/s* in acceleration traces. Some of the recordings were suited for this estimation whereas others were either questionable or purely unsuitable to be considered. This was due to the distance from the bifurcation point where the measurements had taken place. Too far away, and the wave reflection would have attenuated to a less distinct level; too close, and it will arrive very close to the incident pulse wave, creating a blurring effect. Either way, the wave reflections PWV becomes harder to estimate. It is, however, likely for the bifurcation wave reflection PWV to be higher than that of the incident pulse wave. Since the wave reflection arrives later in the cardiac cycle, the vessel wall is more dilated. From its mechanical properties, the vessel wall becomes stiffer as it dilates. Since the incident pulse waves PWV has been proven to increase with increasing arterial stiffness, so would be likely for the bifurcation wave reflection as well. Within several recordings, hints of another wave reflection, probably from the brain, were also present. This wave was, however, not further evaluated due to its discrete appearance in the arterial velocity- and acceleration traces scanlines.

Overall, PWV becomes increasingly more difficult to estimate correctly as the delay between each successive velocity- and acceleration trace decreases. The less distinct the delay is, the faster the pulse wave is traveling through the artery. With ever increasing PWV, the risk of misinterpreting a fast occurring process in the wrong direction becomes reality. The issue is further complicated through possible desynchronization between PWI scanlines, where the sample

points (zero-crossings and peaks) in velocity- and acceleration traces are not aligned properly. Since increased levels of PWV are of considerable interest to detect, they are also more sensitive for incorrect estimations than lower PWV levels. The need for high quality raw data, i.e. high quality ultrafast ultrasound recordings, is thus a high priority. Premature arrival of wave reflections inside the common carotid artery has also been stated to potentially interfere in systolic foot detections in distension waveforms and, thus, heavily affecting PWV estimations [30]. An idea on how to remedy this problem is to exploit some kind of signal separation treatment of the arterial traces, separating the incident- and reflected waves from each other; thus enabling analysis of only the incident wave and its influence on the arterial system.

By studying the subplots of *Figure 4.8* and *Figure 4.11*, any advantages due to some specific methodology or parameter for PWV estimations of the incident pulse wave and bifurcation wave reflection is displayed. Regarding the choice of extracted motion data, *Figure 4.8a* and *Figure 4.11a* show IPS-tracking producing slightly narrower PWV variations than PS-tracking. However, some outliers may still be seen for IPS-tracking in *Table 4.6 – 4.11* as well. Regarding choice of PWV estimation methods, there is no clear pattern in *Figure 4.8b* and *Figure 4.11b* showing whether pulse-echo or scatter plot is preferable. No decisive patterns on if or how local PWV differs in men and women in *Figure 4.8c* and *Figure 4.11c* are also not seen. However, PWV estimations in *Figure 4.8d* clearly show a grouping trend separating values derived from velocity- and acceleration traces. The acceleration traces tend, in most cases, to give lower estimates of the PWV than those of velocity traces. In addition, according to *Table 4.6 – 4.7*, acceleration traces tend to be less prone of giving highly implausible estimations. However, the same pattern is not clearly seen in *Figure 4.11d*.

Acceleration traces display the incident- and reflected pulse waves more qualitatively/visually distinct through PWI than velocity traces. The acceleration peaks are not, strictly speaking, occurring at the arterial diameter foot but, rather, slightly later in the early cardiac upstroke phase. However, they do not occur within reasonable time where wave reflections are normally considered residing. In velocity traces, the incident- and reflected pulse waves are more likely to blur into each other making wave reflection PWV estimations more challenging.

Since the measurements have been performed *in vivo*, variation due to individual variation is undeniable. No human body is the other alike. By sampling on a very small population, eight volunteers between ages 26 – 66 in this case, the outcome is potentially ambiguous. When done on larger populations however, patterns are more likely to appear. Thus, this approach will probably give more unambiguous results when performed as longitudinal studies with follow ups on each volunteer. Then, the immediate individual baseline aspect will be less troublesome when drawing conclusions. All volunteers were considered healthy by a physician attending during the measurements.

5.4 Vascular impedance estimations

The main and final aim of this thesis project, stated in section 1.2, has been to determine vascular impedance inside the right common carotid artery. Since it is the artery supplying blood to the brain, vascular impedance from this sector would show the opposition to blood flow caused by the brain. But, as is shown in section 4.4, its determination has been anything but precise.

Overall, a lot of confusion has existed throughout the process regarding the many definitions of this quantity. In literature, vascular impedance is frequently referred to only as vascular impedance. Since several

definitions of vascular impedance exist, this has been a definite source of misconception and confusion. The total number of impedance definitions is also not totally consistent between sources. As mentioned in section 2.7.1, four definitions for vascular impedance have been referred to in detail in this thesis report; two of which of considerable importance to this thesis project: input- and characteristic impedance.

As described in section 2.7.1, many parallels regarding impedance can be drawn between the vascular system and transmission lines. In fact, many of the definitions regarding vascular impedance are directly transferrable from those regarding transmission lines. There is, however, some miss fitting present in doing so. For transmission lines, characteristic impedance is a key parameter often defined as a fixed valued, non-frequency dependent quantity. Its definition is valid as long as no wave reflections are present within the transmission line or to a very small degree. Transmission lines are, in relation to their thickness, so long that the definition holds true even for some wave reflections. This is, however, not true for the vascular system; in which reflections are always present. Instead, vascular input impedance is considered the impedance definition having immense interest and potential since it takes even considerable wave reflections into account. In literature, the term vascular impedance is often implicitly used to mean vascular input impedance. In practice, however, input impedance is not easily determinable unless performed invasively through pressure- and flow measurements.

Eriksson *et al* [2] showed that characteristic impedance may be used, to some extent, to estimate the vascular input impedance within the arterial system which is illustrated in *Figure 1.4*. This makes their estimations a cross between vascular characteristic- and vascular input impedance, since characteristic impedance is not strictly speaking legal in presence of significant wave reflections. This method, however, shows underestimation in both phase velocity and impedance modulus at low frequencies; down shifting the location of the first impedance

minima, f_{min1} . The underlying reason for this was never fully understood. This also seems to be the case during this thesis project, albeit with additional issues with highly fluctuating phase velocity- and vascular impedance frequency components.

The phase velocity was found far more complicated to estimate correctly than initially anticipated where results often came back as seemingly incorrect or, at least, highly unlikely. This was due to either heavy oscillations between high positive/ high negative phase velocity values in adjacent frequency components or overall low negative phase velocity values in low frequency components. In a way, this method suffers from a similar problem to that of PWV estimation algorithms. They all estimate velocity from change in some quantity over distance; being time occurrence for PWV and phase for phase velocity. Based on a certain set of points, a slope is fitted that determines the velocity in both cases. Based on the appearance of the input impedance modulus pattern in e.g. *Figure 1.4*, phase velocity in e.g. *Figure 1.3*, and thus the fitted slope, should never be negative. Thus, if fitting a slope to less synchronous sample points, the fitting and accompanying slope are incorrectly estimated. When sampling points are widely scattered, the slope will be fitted to that for a nearly flat curve, giving either very high positive or high negative values.

Another problem with the impedance estimations has been the limited cardiac cycles included in the recordings. The signals being analysed in the frequency domain do not contain much energy, potentially jeopardizing the analysis. In an attempt to fix this problem, a compromise was performed by combining one cardiac cycle from each of the 96 diameter traces into two separate signals. Thus, the signals being analysed were $(d_1(t), d_3(t), d_5(t), \dots, d_{93}(t), d_{95}(t))$ and $(d_2(t), d_4(t), d_6(t), \dots, d_{94}(t), d_{96}(t))$. The phase differences between these two signals were then used to estimate the phase velocity for each frequency component. This is, however, not optimal since this combination does not, strictly speaking, create a continuous

signal. Instead, small “jumps” in the signal is created that potentially have an effect on the frequency analysis. To solve this problem all together, new recordings containing more cardiac cycles are needed. The more cardiac cycles that can be included within the recordings, the better. A trade off will, however, be needed due to increased need of data storage space and handling capabilities per recording. An increased number of cardiac cycles would also increase the resolution within the frequency domain, benefitting both the estimations of phase velocity and vascular impedance.

From *Figure 4.13* and *Figure 4.14*, plausible estimations of phase velocity and vascular impedance modulus can be said have been performed during this thesis project. From *Figure 4.13b* and *Figure 4.14b*, plausible characteristic impedance estimations of 50 MNs/m^5 may visually be discerned. But, since this was not the case in most recordings, the projects fall out has not been a complete success. Further work is needed to perfect these estimations *in vivo*.

Furthermore, there is no general agreement on what unit vascular impedance should be given in. As stated in section 2.7.3, vascular impedance may be given in both $\text{dyne}\cdot\text{s}/\text{cm}^3$ and $\text{dyne}\cdot\text{s}/\text{cm}^5$ depending on whether blood flow is considered as linear- or volumic flow respectively. This is not ideal. Another problem is the use of the unit *dyne* in the expression, since it today is considered a long since outdated unit of force. Transformations were thus needed to be performed to relate the results, both from this thesis project and from Eriksson *et al.*, to previous work and estimations performed on laboratory animals and animals. From Eriksson *et al.*, the transformation was performed into units of Ns/m^5 through the following relation:

$$1 \text{ dyne} \cdot \text{s}/\text{cm}^5 = 10^5 \text{ Ns}/\text{m}^5 \quad (5.4.1)$$

This, in combination with results from other sources being scares, makes the procedure more challenging but doable.

Despite being graphically displayable in only some of its definitions; vascular impedance of all forms have their own definite theoretical- and practical meanings and applications. They are all important in their own context. The definitions should, however, be considered more as metaphors rather than analogies to their electrical- and transmission line counterparts. Still, vascular input impedance is undeniably the definition best suited for further pursuit in this field. It is of considerable relevance to the cardiovascular field and has enormous potential in being used in clinical practice. However, graphical representations of vascular input impedance require some knowledge and experience on how to read and interpret them correctly. Characteristic impedance estimations are thus easier to understand and are also highly correlated with PWV.

6. Conclusions

To summarize, this thesis project has been an *in vivo* continuation on the Ph.D. thesis by Eriksson *et al.* [2]. What started out as an intended confirmation of their previously acquired *in vitro* results became a series of advanced and complicated steps including:

- State of the art *in vivo* measurements and beamforming.
- Creation and evaluation of new motion tracking methods.
- Estimations of incident- and reflected PWV:s.
- Determination of vascular input impedance through vascular characteristic impedance.

Vascular impedance and PWV are closely linked in many aspects. Central to non-invasively estimating and determining both quantities are high quality traces of vessel wall motion, which in turn is determined by an equally high quality in motion tracking and ultrasound raw data. Since the pre-existing recordings were found inadequate, new ones had to be taken. Also, due to performance issues with the intended tracking method, new phase based tracking methods had to be designed: PS- and IPS-tracking. Both methods determine the radial vessel movement very well, but IPS-tracking produce more coherent motion traces along the scanlines, and thus the artery.

Today, research oriented physicians have access to many parameters for characterizing blood vessels and the cardiovascular system. A few examples, determinable and estimable through non-invasive ultrasound techniques, are arterial strain, pressure strain elastic modulus, PWV and vascular impedance. No single parameter is, however, perfect. In addition, these parameters are rarely used in every day clinical practice.

PWV is today a commonly estimated quantity for vessel characterization on research level. It may be estimated on both a local- and global scale between separate arteries. Despite having technical requirements being well met, accurate PWV estimations were still proven difficult. Local PWV for the incident pulse wave could vary substantially within and between some volunteers, while giving fairly consistent results in others. The estimations for the bifurcation wave reflection gave even more varying results. Most likely, this is due to imperfections in the recordings and ill fitted slopes to non-synchronous sample points of interest. In cases where PWV estimations gave values of higher variance, the points of interest were also less synchronously placed.

Sometimes being referred to as “*the central problem in hemodynamics*”, vascular impedance has great potential of being used in future healthcare. Its determination is, however, related with some difficulties. The term vascular impedance should be used as a collective term rather than to mean something implicitly specific, as often is today. Since there exists definitions of vascular impedance with various properties and intended uses, it is preferable to announce it. There are also many steps involved in properly determining and estimating vascular impedance. The vascular input impedance determined in this thesis project was difficult to do correctly and was rarely successfully achieved. The probable cause behind this issue has been the limitations set by the recordings; being either too short in terms of included cardiac cycles or other image imperfections. It has, however, been proven possible to estimate vascular input impedance from equations defined for vascular characteristic impedance, to some extent, with wave reflections present in the system. Like for Eriksson *et al.* [2] was vascular impedance occasionally underestimated for low frequencies and, thus, down shifting the first local minima, f_{min1} . Despite its long historical background, vascular impedance is rarely pursued in practice; even on research level. Vascular input impedance has frequently been determined invasively *in vivo* in both humans and

animals. Non-invasive measurements, however, are scarcer. Furthermore, the field is far from standardized. Many of its definitions and guidelines are still being debated amongst physicians, cardiologists and biomedical engineers to this day. Considerable research is still needed to ease the development for this potentially very useful quantity for cardiovascular characterization to be applied in everyday clinical practice.

Bibliography

1. WHO. *Cardiovascular diseases (CVDs)*. 2017 [cited 2018 - 11 - 25]; Available from: [http://www.who.int/news-room/fact-sheets/detail/cardiovascular-diseases-\(cvds\)](http://www.who.int/news-room/fact-sheets/detail/cardiovascular-diseases-(cvds)).
2. Eriksson, A., *Development and evaluation of non-invasive ultrasonic methods for arterial characterization*. 1999, Lund University: Department of Electrical Measurements, Lund, Sweden.
3. Sjöstrand, S. and A. Widerström, *Design and Fabrication of Ultrasound Phantoms to Identify the Actuator of Arterial Wall Longitudinal Movement*. 2015, Lund University: Department of Biomedical Engineering, Lund, Sweden.
4. Meizra, B., *Development of Vessel Phantoms for Ultrasound Methods*. 2018, Lund University: Department of Biomedical Engineering, Lund, Sweden.
5. Hoskins, P., K. Martin, and A. Thrush, *Diagnostic ultrasound: physics and equipment*. Second ed. Cambridge Medicine. 2011, University Printing House, United Kingdom: Cambridge University Press.
6. Maccallum, K. *Pros and cons of two popular Ultrasound signal processing techniques*. 2018 [cited 2018- 11- 09]; Available from: <https://starfishmedical.com/2015/02/19/pros-cons-two-popular-ultrasound-signal-processing-techniques/>.
7. Desailly, Y., et al., *Sono-activated ultrasound localization microscopy*. Applied Physics Letters, 2013. **103**(17).
8. Bercoff, J., *Ultrasound Imaging - Medical Applications*, O. Minin, Editor. 2011, InTech.
9. Entekin, R.R., et al., *Real-time spatial compound imaging: Application to breast, vascular, and musculoskeletal ultrasound*. Seminars in Ultrasound Ct and Mri, 2001. **22**(1): p. 50-64.
10. Saltzman, W.M., *Biomedical Engineering: Bridging Medicine And Technology*. Second ed. 2015, University Printing House, United Kingdom: Cambridge University Press.

11. LumenLearning. *Blood Flow, Blood Pressure and Resistance* 2018 [cited 2018 - 12 - 14]; Available from: <https://courses.lumenlearning.com/suny-ap2/chapter/blood-flow-blood-pressure-and-resistance-no-content/>.
12. AmericanDiagnosticCorporation. *History of the Sphygmomanometer*. 2018 [cited 2018 - 10 - 16]; Available from: <https://www.adctoday.com/learning-center/about-sphygmomanometers/history-sphygmomanometer>.
13. Cedars-Sinai. *Endothelial Function Testing*. 2018 [cited 2018 - 10 - 16]; Available from: <https://www.cedars-sinai.org/programs/heart/clinical/womens-heart/services/endothelial-function-testing.html>.
14. Larsson, M., et al., *Strain assessment in the carotid artery wall using ultrasound speckle tracking: validation in a sheep model*. *Physics in Medicine and Biology*, 2015. **60**(3): p. 1107-1123.
15. Kohen A. J., Krouchkov N., and V.M. E., *The concept of Vascular Impedance revisited*. *International Journal of Biomedical Engineering and Technology*, 2011. **6**(2).
16. Nichols, W.W. and M.F. O'Rourke, *McDonald's Blood Flow In Arteries*. Fifth Edition ed. 2005: Hodder Arnold.
17. Glover, J.D., M.S. Sarma, and T.J. Overbye, *Power System Analysis and Design*. Fifth ed. 2012, Stamford, USA: CENGAGE Learning.
18. van de Vosse, F.N. and M.E.H. van Dongen, *Cardiovascular Fluid Mechanics - lecture notes*. 1998, Eindhoven University of Technology.
19. EncyclopædiaBritannica. *Dyne*. 1999 [cited 2018 - 10 - 28]; Available from: <https://www.britannica.com/science/dyne>.
20. van de Vosse, F.N. and N. Stergiopoulos, *Pulse Wave Propagation in the Arterial Tree*. *Annual Review of Fluid Mechanics*, Vol 43, 2011. **43**: p. 467-499.
21. *terminal impedance*. 2017 [cited 2018 - 11 - 07]; Available from: https://link.springer.com/referenceworkentry/10.1007%2F1-4020-0613-6_19367.
22. Katz, L.N., *Observations on the external work of the isolated turtle heart*. *Am. J. Physiol.*, 1931. **99**: **579-97**.
23. Bramwell, J.C. and A.V. Hill, *Velocity of transmission of pulse wave and elasticity of arteries*. *Lancet*, 1922. **1**: **891-2**.
24. Albinsson, J., et al., *Iterative 2D Tissue Motion Tracking in Ultrafast Ultrasound Imaging*. *Applied Sciences*, 2018. **8**(5).

25. Dipartimento di Ingegneria dell'Informazione, U.d.S.d.F. *ULA-OP 256 System*. 2012; Available from: <https://www.dinfo.unifi.it/vp-261-ula-op-256-system.html>.
26. ResearchGate. *Alessandro Ramalli*. 2018 [cited 2018 - 12 - 05]; Available from: https://www.researchgate.net/profile/Alessandro_Ramalli.
27. Luo, J.W., R.X. Li, and E.E. Konofagou, *Pulse Wave Imaging of the Human Carotid Artery: An In Vivo Feasibility Study*. Ieee Transactions on Ultrasonics Ferroelectrics and Frequency Control, 2012. **59**(1): p. 174-181.
28. Pereira, T., C. Correia, and J. Cardoso, *Novel Methods for Pulse Wave Velocity Measurement*. Journal of Medical and Biological Engineering, 2015. **35**(5): p. 555-565.
29. Apostolakis, I.Z., S.D. Nandlall, and E.E. Konofagou, *Piecewise Pulse Wave Imaging (pPWI) for Detection and Monitoring of Focal Vascular Disease in Murine Aortas and Carotids In Vivo*. Ieee Transactions on Medical Imaging, 2016. **35**(1): p. 13-28.
30. Hermeling, E., et al., *Confluence of incident and reflected waves interferes with systolic foot detection of the carotid artery distension waveform*. Journal of Hypertension, 2008. **26**(12): p. 2374-2380.